DIFFUSION BLEND: INFERENCE-TIME MULTI-PREFERENCE ALIGNMENT FOR DIFFUSION MODELS

Anonymous authors
Paper under double-blind review

ABSTRACT

Reinforcement learning (RL) algorithms have been used recently to align diffusion models with downstream objectives such as aesthetic quality and text-image consistency by fine-tuning them to maximize a single reward function under a fixed KL regularization. However, this approach is inherently restrictive in practice, where alignment must balance multiple, often conflicting objectives. Moreover, user preferences vary across prompts, individuals, and deployment contexts, with varying tolerances for deviation from a pre-trained base model. We address the problem of inference-time multi-preference alignment: given a set of basis reward functions and a reference KL regularization strength, can we design a fine-tuning procedure so that, at inference time, it can generate images aligned with any user-specified linear combination of rewards and regularization, without requiring additional fine-tuning? We propose Diffusion Blend, a novel approach to solve inference-time multi-preference alignment by blending backward diffusion processes associated with fine-tuned models, and we instantiate this approach with three algorithms: DB-MPA for multi-reward alignment, DB-KLA for KL regularization control, and DB-MPA-LS for approximating DB-MPA without additional inference cost. Extensive experiments show that Diffusion Blend algorithms consistently outperform relevant baselines and closely match the performance of individually fine-tuned models, enabling efficient, user-driven alignment at inference-time.

1 INTRODUCTION

Diffusion models, such as Imagen (Saharia et al., 2022a), DALL·E (Ramesh et al., 2022), and Stable Diffusion (Rombach et al., 2022), have demonstrated remarkable capabilities in high-fidelity image synthesis from natural language prompts. However, these models are typically trained on large-scale datasets and are not explicitly optimized for downstream objectives such as semantic alignment, aesthetic quality, or user preference. To address this gap, recent works have proposed reinforcement learning (RL) for aligning diffusion models with task-specific reward functions (Uehara et al., 2024a; Fan et al., 2023; Black et al., 2024), where the core idea is to fine-tune a pre-trained model to maximize a reward, while constraining the update to remain close to the original model via a Kullback–Leibler (KL) regularization. The KL regularization term prevents reward overoptimization (reward hacking), and preserves desirable properties of the pre-trained model (Ouyang et al., 2022; Rafailov et al., 2023) such as sample diversity and visual fidelity (Fan et al., 2023; Uehara et al., 2024b).

While RL fine-tuning has improved alignment in diffusion models, it typically assumes a fixed reward function and regularization weight. This assumption is restrictive in practice, where alignment must balance multiple, often conflicting objectives, such as aesthetics and prompt fidelity, and user preferences vary across prompts, individuals, and deployment contexts. Static fine-tuning with fixed reward combinations cannot accommodate this variability without retraining separate models for each configuration (Wang et al., 2024b; Rame et al., 2023; Lee et al., 2024). Moreover, once trained, the trade-offs are fixed, precluding post-hoc adjustment. Similar issues arise with KL regularization: insufficient regularization causes reward hacking, while excessive regularization impedes alignment (Uehara et al., 2024b; Liu et al., 2024). In practice, both reward and regularization weights are tuned via grid search, incurring significant computational cost and limiting flexibility.

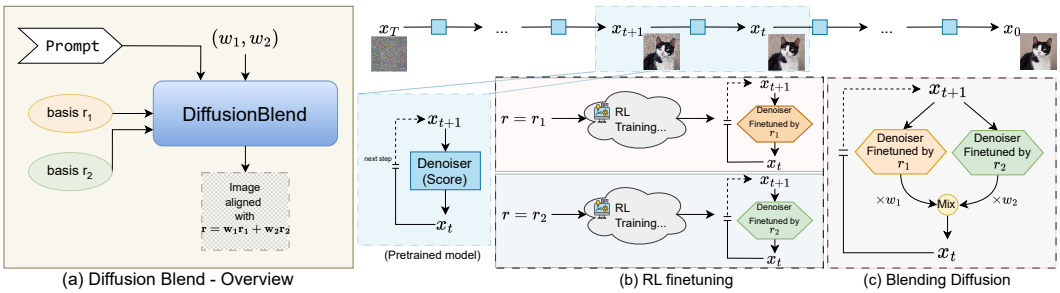

Figure 1: (a). Overview of our Diffusion Blend - Multi Preference Alignment (DB-MPA) Algorithm. Given basis reward functions and any user preference weights $w = (w_1, w_2)$, DB-MPA generates images aligned with combined reward $r(w) = w_1 r_1 + w_2 r_2$. (b) During the fine-tuning stage, DB-MPA gets an RL fine-tuned model corresponding to each reward function. (c) During the inference time, DB-MPA blends (mixes) the backward diffusion corresponding to each fine-tuned model according to the user-specified preference w.

These limitations motivate the need for a more flexible approach: **inference-time multi-preference alignment**, where the user specifies their preference vector, i.e., weights over a set of basis reward functions such as alignment, aesthetics, or human preference, along with a desired regularization strength that controls deviation from the pre-trained model. Crucially, this alignment must occur without any additional fine-tuning or extensive computation at inference time, which is essential for real-time and resource-constrained settings. Unlike trial-and-error prompt tuning, the ideal solution should offer a principled and computationally efficient solution that can achieve Pareto-optimal trade-offs across multiple preferences. This motivates us to address the following questions:

Given a set of basis reward functions $(r_i)_{i=1}^m$ and a basis KL regularization weight α, can we design a fine-tuning procedure such that when the user specifies their reward or regularization preferences through parameters w and λ at inference time, the model generates images aligned with the linear reward combination $r(w) = \sum_{i=1}^m w_i r_i$ and regularization weight $\alpha(\lambda) = \alpha/\lambda$, without requiring additional fine-tuning? In this work, we answer this question affirmatively and provide constructive solutions to it. Our main contributions are the following:

- We theoretically show that the backward diffusion process corresponding to the diffusion model aligned with reward function $r(w)$ and regularization weight α can be expressed as the backward diffusion process corresponding to the pre-trained model with an additional control term that depends on $r(w)$. We propose an approximation result for this control term, which enables us to express it using the control terms corresponding to fine-tuned diffusion models for the basis reward functions $(r_i)_{i=1}^m$. We also obtain a similar approximation result corresponding to the regularization weight α.
- Leveraging the theoretical results we developed, we propose Diffusion Blend - Multi-Preference Alignment **(DB-MPA)** algorithm, a novel approach that will blend the backward diffusion processes corresponding to the basis reward functions appropriately to synthesize a new backward diffusion process during inference-time that will generate images aligned with the reward $r(w)$, where w is specified by the user during the inference-time. Using the same approach, we also propose Diffusion Blend - KL Alignment **(DB-KLA)** algorithm that will generate images aligned with a reward function r and regularization weight α/λ, where λ is specified by the user during the inference time. To reduce the computational overhead associated with DB-MPA, we propose Diffusion Blend - Multi-Preference Alignment- LoRA Sampling **(DB-MPA-LS)** algorithm that addresses the increased inference time issue while maintaining similar performance.
- We provide extensive experimental evaluations using the Stable Diffusion (Rombach et al., 2022) baseline model, multiple basis reward functions, regularization weights, standard prompt sets, and demonstrate that our diffusion blend algorithms outperform multiple relevant baseline algorithms, and often achieve a performance close to the empirical upper bound obtained by an individually fine-tuned model for specific w and λ.

2 Related Work

Finetuning-based algorithms: Prior works align diffusion models via reward-guided finetuning. Rewards-in-context (Yang et al., 2024) conditions on multiple reward types, DRaFT (Clark et al., 2024) uses weighted combinations during training, and (Hao et al., 2023) applies RL with alignment–aesthetic trade-offs. Parrot (Lee et al., 2024) leverages prompt expansion, while Calibrated

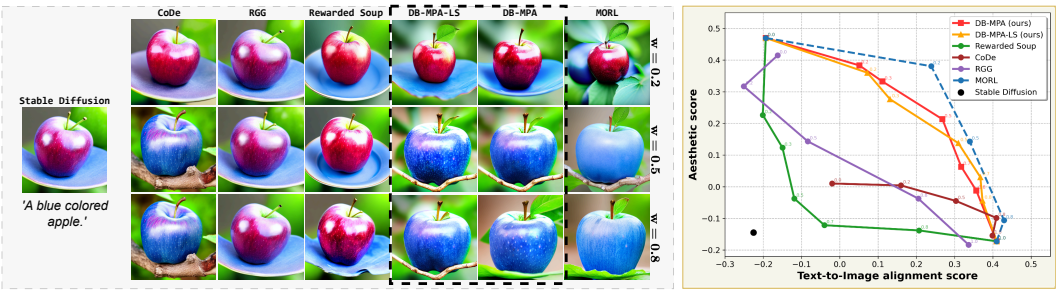

(a) Visual Comparison (b) Pareto front

Figure 2: Comparison of DB-MPA with baselines: Stable Diffusion v1.5 (Rombach et al., 2022), CoDe (Singh et al., 2025), RGG (Chung et al., 2023), rewarded soup (RS) (Rame et al., 2023), and MORL (Roijers et al., 2013). Note that MORL is included only to illustrate the maximum achievable performance by an oracle algorithm. See section 2 for details. For arbitrary preference weight w, algorithms generate images aligned with $r(w) = wr_1 + (1-w)r_2$, where r_1 is text-to-image alignment and r_2 is aesthetics. **(a)** Images for $w \in \{0.2, 0.5, 0.8\}$. **(b)** Pareto-front comparison. DB-MPA significantly outperforms baselines and approaches the MORL upper bound.

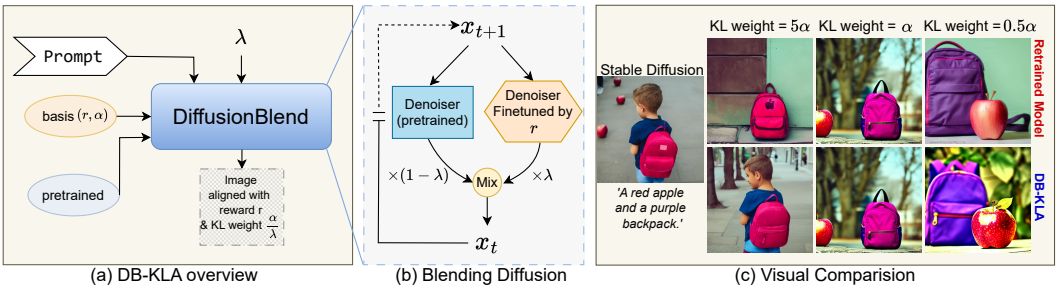

(a) DB-KLA overview (b) Blending Diffusion (c) Visual Comparision

Figure 3: **(a)** Overview of our Diffusion Blend-KL Alignment (DB-KLA) Algorithm. Given an RL fine-tuned model for reward r with KL weight α, DB-KLA generates images aligned with KL weight α/λ for any user-specified modification factor λ. **(b)** During inference, DB-KLA blends the backward diffusion of the fine-tuned and pretrained models according to λ, which can be larger than 1. **(c)** Visual comparisons with λ-specific RL retrained models using text-to-image-alignment reward and $\lambda \in \{0.2, 1.0, 2.0\}$. DB-KLA achieves smooth control by adjusting the effective distance from the pre-trained model via λ, generating images similar to λ-specific RL models without additional fine-tuning.

DPO (Lee et al., 2025) aggregates multiple reward models. Rewarded Soup (RS) (Rame et al., 2023) is closest to us, linearly combining parameters from reward-specific models, whereas our DB-MPA blends backward diffusion trajectories in a principled way.

Guidance algorithms: Gradient-based methods (Chung et al., 2023; Yu et al., 2023; Song et al., 2023; Bansal et al., 2023; He et al., 2024; Ye et al., 2024) add reward gradients at each reverse diffusion step, and can handle multiple objectives (Han et al., 2023; Kim et al., 2025; Ye et al., 2024). They require differentiable rewards and Tweedie-based approximations (Efron, 2011), leading to noise and high cost. Gradient-free methods instead generate multiple candidates and select high-reward samples (Mudgal et al., 2024; Gui et al., 2024; Beirami et al., 2024), or use particle/value-guided search (Li et al., 2024; Singhal et al., 2025; Singh et al., 2025). These avoid gradients but demand heavy sampling and reward access.

Multi-Objective RL (MORL): Approaches (Roijers et al., 2013; Yang et al., 2019; Zhou et al., 2022; Rame et al., 2023) fine-tune a separate model for each preference or regularization weight. While theoretically optimal, inference-time RL is infeasible; even covering the weight space requires exponentially many models. We thus treat MORL only as an oracle baseline.

Multi-preference alignment in LLMs: Works such as (Rame et al., 2023; Jang et al., 2023; Shi et al., 2024; Wang et al., 2024b; Guo et al., 2024; Zhong et al., 2024b; Wang et al., 2024a) extend RL finetuning to LLMs. For KL-regularized alignment, DeRa (Liu et al., 2024) controls alignment by combining logits from aligned and reference models. Our diffusion blend methods are inspired by these but introduce inference-time preference alignment specifically for diffusion models.

LoRA composition for image generation: Recent work on multi-concept fusion in diffusion models (Zhong et al., 2024a; Zou et al., 2025) focuses on composing pretrained LoRA modules using

fixed, heuristic scheduling to mitigate degradation when multiple concepts are combined. In contrast, our DB-MPA framework blends reward-aligned diffusion trajectories, enabling principled and interpretable trade-offs rather than heuristic mixing.

3 Preliminaries and Problem Formulation

Diffusion model and pre-training: A diffusion model (Ho et al., 2020; Song et al., 2021) approximates an unknown data distribution p_{data} by an iterative approach. It consists of a forward process and a backward process. In the forward process, a clean sample from the data distribution p_{data} is progressively corrupted by adding Gaussian noise at each timestep, ultimately transforming the data distribution into pure noise. The reverse process involves training a denoising neural network to iteratively remove the added noise and reconstruct samples from the original data distribution. The forward process is typically represented by the stochastic differential equation (SDE), $\mathrm{d}x_t = -\frac{1}{2}\beta(t)x_t\mathrm{d}t + \sqrt{\beta(t)}\mathrm{d}w_t,\ \forall t \in [0, T]$,

where $x_0 \sim p_{\text{data}}$, $\beta(t)$ is a predefined noise scheduling function, and w_t represents a standard Wiener process. The reverse process of this SDE is given by (Anderson, 1982; Song et al., 2021)

$$\mathrm{d}x_t = [-\frac{1}{2}\beta(t)x_t - \beta(t)\nabla_{x_t}\log p_t(x_t)]\mathrm{d}t + \sqrt{\beta(t)}\mathrm{d}w_t,\ \forall t \in [T, 0], \tag{1}$$

where p_t denotes the marginal probability distribution of x_t, x_T is sampled according to a standard Gaussian distribution, and $\nabla_{x_t}\log p_t(x_t)$ represents the *score function* that guides the reverse process. Since the marginal density p_t is unknown, the score function is estimated by a neural network s_θ through minimizing score-matching objective (Song et al., 2021) given by the optimization problem, $\arg\min_\theta\ \mathbb{E}_{t\sim U[0,T]}\mathbb{E}_{x_0\sim p_{\text{data}}}\mathbb{E}_{x_t\sim p_t(\cdot|x_0)}\left[\lambda(t)\left\|\nabla_{x_t}\log p_t(x_t|x_0) - s_\theta(x_t, t)\right\|^2\right]$, where $s_\theta(x_t, t)$ is a neural network parameterized by θ that approximates the score function and $\lambda(t)$ is a weighting function. In the following, we denote the pre-trained diffusion model by the (backward) SDE

$$\mathrm{d}x_t = f^{\text{pre}}(x_t, t)\mathrm{d}t + \sigma(t)\mathrm{d}w_t,\ \forall t \in [T, 0], \tag{2}$$

where $f^{\text{pre}}(x_t, t)$ denotes the term $[-\frac{1}{2}\beta(t)x_t - \beta(t)\nabla_{x_t}\log p_t(x_t)]$ in eq. (1), and $\sigma(t)$ denotes the noise scheduling function. We will use p_t^{pre} to denote the distribution of x_t according to the pre-trained diffusion model given by the backward SDE in eq. (2).

RL fine-tuning of pre-trained diffusion model: Diffusion models are pre-trained to learn the score function, and are not trained to additionally maximize downstream rewards such as aesthetic score. Aligning a pre-trained diffusion model with a given reward function $r(\cdot)$ can be formulated as the optimization problem $\max_{p_0}\mathbb{E}_{x_0\sim p_0}[r(x_0)]$, with the initialization p_0^{pre}.

However, this can lead to reward over-optimization, disregarding the qualities of data-generating distribution p_0^{pre} learned during the pre-training (Fan et al., 2023). To avoid this issue, similar to the LLM fine-tuning (Ouyang et al., 2022), a KL-divergence term between the pre-trained and fine-tuned models is included as a regularizer to the RL objective (Fan et al., 2023), resulting in the *diffusion model alignment problem*:

$$\max_{p_0}\ \mathbb{E}_{x_0\sim p_0}[r(x_0)] - \alpha\mathrm{KL}(p_0\|p_0^{\text{pre}}), \tag{3}$$

where α is the KL regularization weight. Since directly evaluating KL divergence between p_0 and p_0^{pre} is challenging, it is to upperbounded it by the sum of the KL divergences between the conditional distributions at each step (Fan et al., 2023), resulting in the fine-tuning objective

$$\max_{(p_t)_{t=T}^0}\ \mathbb{E}[r(x_0) - \alpha\sum_{t=T}^{1}\mathrm{KL}(p_t(\cdot|x_t)\|p_t^{\text{pre}}(\cdot|x_t))], \tag{4}$$

where the expectation is taken w.r.t. $\Pi_{t=T}^1 p_t(x_{t-1}|x_t)$, and $x_T \sim p_T$. While the optimization is over a sequence of distributions, $(p_t)_{t=T}^0$, in practice, we learn only the score function parameter θ which will induce the distributions p_t as p_t^θ. We assume that this fine-tuning objective will solve eq. (3) approximately, which will result in a fine-tuned model aligned with r and α. Similar to the notation in eq. (2), we represent the backward diffusion process corresponding to this fine-tuned model as

$$\mathrm{d}x_t = f^{(r,\alpha)}(x_t, t)\mathrm{d}t + \sigma(t)\mathrm{d}w_t,\ \forall t \in [T, 0], \tag{5}$$

where $f^{(r,\alpha)}$ depends on r, α. The exact form of $f^{(r,\alpha)}$ is derived in proposition 1.

The fine-tuning problem in eq. (4) is typically solved using RL by formulating it as an entropy-regularized Markov Decision Process (MDP) (Fan et al., 2023; Uehara et al., 2024a). The state $\mathcal{S}$ and action $\mathcal{A}$ spaces are defined as the set of all images $\mathcal{X}$. The transition dynamics at each step t is deterministic, $P_t(s_{t+1} \mid s_t, a_t) = \delta(s_{t+1} = a_t)$. The reward function is non-zero only for $t = T$ and $r(s_t) = 0, \forall t \in \{0, \dots, T-1\}$. The policy $\pi_t : \mathcal{S} \to \Delta(\mathcal{A})$ is modeled as a Gaussian distribution, matching with the discretization of the reverse process given in eq. (2). To align with the diffusion model notation, we define $s_t = x_{T-t}$, $a_t = x_{T-t-1}$, and $\pi_t(a_t|s_t) = p_{T-t-1}(x_{T-t-1}|x_{T-t})$. The initial distribution of the state $s_0 = x_T$ is standard Gaussian.

Problem: Inference-Time Multi-Prefence Alignment: The main issue with the standard RL fine-tuning (eq. (3)-eq. (4)) is that the fine-tuned model is optimized for a fixed (r, α), and the model is unchangeable after fine-tuning. So, it is not possible to generate optimally aligned data samples for another reward r or regularization weight α at inference time. To address this problem, we follow the standard multi-objective RL formalism (Yang et al., 2019; Zhou et al., 2022), where we consider a multi-dimensional reward $(r_1, r_2, \dots, r_m)$ and assume that the reward is represented by a linear scalarization $r(w) = \sum_{i=1}^m w_i r_i, w \in \Delta_m$, where Δ_m is the m-dimensional simplex. At inference time, the user communicates their preferences by specifying the reward function weight w. We also assume that the user specifies a regularization modification factor λ to propose an effective regularization weight $\alpha(\lambda) = \alpha/\lambda$. In this paper, we address the following problem:

How do we solve the alignment problem in eq. (3) *for arbitrary reward function $r(w)$ and regularization weight $\alpha(\lambda)$ without additional fine-tuning at inference time? Note that w and λ are user-specified values at inference time.*

4 Diffusion Blend Algorithm

The alignment problem in eq. (3) is the same as the one used for LLMs (Rafailov et al., 2023; Liu et al., 2024). Recent results in LLMs, especially those that use the direct preference optimization approach (Rafailov et al., 2023), have leveraged the following closed-form solution to eq. (3) to develop alignment algorithms:

$$p^{\mathrm{tar}}(x_0) = p^{\mathrm{pre}}(x_0) \cdot \exp\big(r(x_0)/\alpha\big) \;/\; Z \;, \tag{6}$$

where Z is a normalization constant. However, in the case of diffusion models, directly sampling from p^{tar} is infeasible for two reasons. First, computing Z is intractable, as it requires evaluating an integral over a high-dimensional continuous space. Second, unlike in the case of LLM where $p^{\mathrm{pre}}(x)$ for any token x is available at the output layer of the LLM, diffusion models do not offer an explicit way to evaluate $p^{\mathrm{pre}}(x)$ for an arbitrary x. Instead, we can only sample from p^{pre} by running a backward SDE. In other words, we will not be able to directly sample from p^{tar} by tilting p^{pre} as given in eq. (6), even if the value of Z is known. RL fine-tuning achieves sampling from p^{tar} by learning a model that can synthesize the backward diffusion specified by $f^{(r,\alpha)}$. However, this would suggest an extensive RL fine-tuning for different values of w and λ in $r(w)$ and $\alpha(\lambda)$. To address this, we describe an interesting mapping between f^{pre} and $f^{(r,\alpha)}$, which we will then exploit to solve the inference-time multi-preference alignment problem without naive extensive fine-tuning.

Let $x_0^{\mathrm{pre}} \sim p^{\mathrm{pre}}(\cdot)$, $x_0^{\mathrm{tar}} \sim p^{\mathrm{tar}}(\cdot)$, and $(\epsilon_t)_{t=1}^T$ be an independent, zero mean Gaussian noise sequence with probability distribution p_{ϵ_t}, i.e., $\epsilon_t \sim p_{\epsilon_t}(\cdot)$. Consider the forward noise processes $x_t^{\mathrm{pre}} = x_0^{\mathrm{pre}} + \epsilon_t$ and $x_t^{\mathrm{tar}} = x_0^{\mathrm{tar}} + \epsilon_t$, and let p_t^{pre} and p_t^{tar} be the marginal distributions of x_t^{pre} and x_t^{tar}, respectively. As standard in the diffusion model literature (Song et al., 2021; Ho et al., 2020), we assume that under the forward noise process, the distributions of x_T^{pre} and x_T^{tar} are Gaussian. Let $p_{0|t}^{\mathrm{pre}}$ denote the conditional distribution of x_0^{pre} given x_t^{pre}. Then, we have the following result.

Proposition 1. *Let $f^{(r,\alpha)}$ and f^{pre} be as specified in eq.* (5) *and eq.* (2)*, respectively. Then, $f^{(r,\alpha)}(x_t, t) = f^{\mathrm{pre}}(x_t, t) - \beta(t) u^{(r,\alpha)}(x_t, t)$, where*

$$u^{(r,\alpha)}(x_t, t) = \nabla_{x_t} \log \, \mathbb{E}_{x_0 \sim p_{0|t}^{\mathrm{pre}}(\cdot|x_t)} \left[\exp\left(\frac{r(x_0)}{\alpha} \right) \right]. \tag{7}$$

Remark 1. We prove proposition 1 following the SDE interpretation of diffusion models (Song et al., 2021), and by showing that two SDEs initialized at time $t = 0$ at p^{pre} and p^{tar}, and sharing the same forward noise injection process, can be reversed similarly. In particular, we show that

the key parameters of the corresponding two reverse SDEs remain unchanged, except that the latter includes an additional control term $u^{(r,\alpha)}$ in the score function. We note that (Uehara et al., 2024b) derives a similar result by analyzing the RL objective in eq. (4) and leveraging results from stochastic optimal control. In contrast, our approach analyzes the original alignment objective in eq. (3) and derives a simpler, first-principles proof without relying on stochastic optimal control theory, under the standard mild assumption that for large T, the terminal distribution of both forward SDEs is Gaussian.

We now consider an approximation $\bar{u}^{(r,\alpha)}$ to $u^{(r,\alpha)}$, motivated by the Jensen gap approximation idea that has been successfully utilized in algorithms for noisy image inverse problems (Chung et al., 2023; Rout et al., 2023; 2024). Let x be a random variable with distribution p. For a nonlinear function f, the Jensen gap is defined as $\mathbb{E}[f(x)] - f(\mathbb{E}[x])$. In our case, we interchange the expectation $\mathbb{E}[\cdot]$ and the nonlinear function $\exp(\cdot)$ in $u^{(r,\alpha)}$ to obtain the following approximation:

$$u^{(r,\alpha)}(x,t) = \bar{u}^{(r,\alpha)}(x,t) + \Delta^{(r,\alpha)}(x,t), \quad \text{where} \quad \bar{u}^{(r,\alpha)}(x,t) = \nabla_x \mathbb{E}_{x_0 \sim p^{\mathrm{pre}}_{0|t}(\cdot|x)} \left[\frac{r(x_0)}{\alpha} \right]. \tag{8}$$

We also prove an upper-bound on the approximation error $\Delta^{(r,\alpha)}(x,t)$ in eq. (8) in the appendix A.2. Beyond validating our approach, our theoretical analysis offers practical insights into when approximation errors are likely to be small and provides a broader perspective on related methods, naturally recovering Uehara et al. (2024b)'s assumption as a special zero-error case. Refer appendix A.2 for more details.

The key motivation behind the approximation in eq. (8) is that we can now leverage the linearity of expectation available in $\bar{u}^{(r,\alpha)}$ to approximate $f^{(r(w),\alpha(\lambda))}$ in terms of $f^{(r_i,\alpha)},\ i = 1, \ldots, m$.

Lemma 1. *Let $f^{(r,\alpha)}$ be as specified in eq.* (5)*. Then, we have*

$$f^{(r(w),\alpha)}(x_t,t) = \sum_{i=1}^{m} w_i f^{(r_i,\alpha)}(x_t,t) + \beta(t) \left(\sum_{i=1}^{m} w_i \Delta^{(r_i,\alpha)}(x,t) - \Delta^{(r(w),\alpha)}(x,t) \right), \tag{9}$$

$$f^{(r,\alpha(\lambda))}(x_t,t) = (1-\lambda) f^{\mathrm{pre}}(x_t,t) + \lambda f^{(r,\alpha)}(x_t,t) + \beta(t) \left(\lambda \Delta^{(r,\alpha)}(x,t) - \Delta^{(r,\alpha(\lambda))}(x,t) \right). \tag{10}$$

Using the result in lemma 1, we now introduce our diffusion blend algorithms, with pseudo code provided in appendix B.2.

Diffusion Blend-Multi-Preference Alignment (DB-MPA) Algorithm: Our goal is to solve the alignment problem in eq. (3) for an arbitrary reward function $r(w)$ with user-specified parameter w, without additional fine-tuning at inference time. This is equivalent to obtaining the diffusion term $f^{(r(w),\alpha)}$ and running the backward SDE in eq. (5). At the fine-tuning stage (before deployment), we independently fine-tune the pre-trained model for each reward $(r_i)_{i=1}^m$ with fixed α, obtaining m RL fine-tuned models $(\theta_i^{\mathrm{rl}})_{i=1}^m$ by solving the fine-tuning objective in eq. (3). At inference, we use lemma 1 to approximate $f^{(r(w),\alpha)}(x_t,t) \approx \sum_{i=1}^m w_i f^{(r_i,\alpha)}(x_t,t)$, where each $f^{(r_i,\alpha)}$ is computed using the RL fine-tuned model θ_i^{rl}. We then generate samples by running the backward SDE in eq. (5).

Diffusion Blend-KL Alignment (DB-KLA) Algorithm: Our goal is to solve the alignment problem in eq. (3) for an arbitrary regularization weight $\alpha(\lambda)$ with user-specified parameter λ, without additional fine-tuning at inference time. This is equivalent to running the backward diffusion in eq. (5) with $f^{(r,\alpha(\lambda))}$. At fine-tuning, we fine-tune the pre-trained model for reward r and regularization weight α, obtaining RL fine-tuned model θ^{rl} from θ^{pre}. At inference, we use lemma 1 to approximate $f^{(r,\alpha(\lambda))}(x_t,t) \approx (1-\lambda) f^{\mathrm{pre}}(x_t,t) + \lambda f^{(r,\alpha)}(x_t,t)$, where f^{pre} and $f^{(r,\alpha)}$ are computed using θ^{pre} and θ^{rl}, respectively. We then generate samples by running the backward SDE in eq. (5).

4.1 Inferrence time efficient variant

While DB-MPA and DB-KL successfully achieve reward alignment through score merging, this approach requires evaluating all m diffusion models at each denoising step, resulting in $m\times$ computational overhead during inference. To address this limitation, we propose DB-MPA-with-LoRA-

Sampling (DB-MPA-LS), a novel algorithm that approximates the score merging process by randomly sampling reward fine-tuned LoRA adapters at each denoising step with probabilities proportional to their assigned weights. This approach reduces the inference cost to that of the original pre-trained Stable Diffusion model, eliminating the multiplicative overhead inherent in inference-time realignment methods, including our DB-MPA and existing LLM variants Liu et al. (2024); Shi et al. (2024). Note that this sampling approximation cannot be applied to DB-KL since the KL reweighting terms may be negative. The key insight is that unlike LLM realignment which mixes probabilities over discrete and finite tokens, diffusion models operate through continuous stochastic processes where the noise-adding nature enables a different mathematical treatment, which we show by the following proposition.

Proposition 2. *For the Lipschitz continuous functions f_1 and f_2, the following two SDE have the same marginal probability $p_{X_t^1} = p_{X_t^2}$ for $\forall\ t \in [0, T]$. SDE 1 is $dX_t^1 = (af_1(X_t^1) + (1 - a)f_2(X_t^1))dt + \sigma(t)d\omega_t$, with $X_0 \sim p_0$, $t \in [0, T]$, and $\{\omega_t\}$ being the Winner process. SDE 2 is $dX_t^2 = (Y_t f_1(X_t^2) + (1 - Y_t)f_2(X_t^2))dt + \sigma(t)d\omega_t$, with $X_0 \sim p_0$, $t \in [0, T]$, and $\{\omega_t\}$ being the Winner process, where Y_t is a Bernoulli random variable with probability a to be 1 and probability $1 - a$ to be 0, and Y_t is independent of $\{X_t^2\}_t$ and Y_s for any $s \neq t$.*

Remark 2. Without loss of generality, we present the theoretical result for the two-reward case ($m = 2$), as the extension to arbitrary finite m rewards follows straightforwardly by replacing the Bernoulli variable with a categorical random variable. Details of the proof are in appendix A.4.

5 Experiments

In this section, we present comprehensive experimental evaluations that demonstrate the superior performance of our DB-MPA and DB-KLA algorithms compared to the baseline models. The code is available at `https://anonymous.4open.science/r/iboayewg`.

Reward models. We use four reward models in our experiments: (i) *ImageReward* (Xu et al., 2024), which measures the text-image alignment and is used in its original form; (ii) *VILA* (Ke et al., 2023), which measures the aesthetic quality of generated images and outputs in $[0, 1]$, is rescaled to $[-2, 2]$ via $r \mapsto 4r - 2$ to normalize its influence relative to other rewards; and (iii) *PickScore* (Kirstain et al., 2023), which measures how well an image generated from a text prompt aligns with human preferences, is shifted by -19 to match the scale of other rewards. (iv) We further test our algorithm on a *JPEG compressibility* reward, which opposes aesthetics by favoring smooth images, enabling analysis of adversarial alignment.

Baselines: We compare the performance of our algorithms with the following baseline algorithms: (i) Rewarded Soup (RS) (Rame et al., 2023), (ii) CoDe (Singh et al., 2025), a gradient-free guidance algorithm with look-ahead search, where we use $N = 20$ particles for the search and $B = 5$ look-ahead steps. (iii) Reward gradient-based guidance (RGG) (Chung et al., 2023; Kim et al., 2025), and (iv) Multi-Objective RL (MORL) (Rame et al., 2023; Wu et al., 2023). Details of these baselines are given in appendix B.1. Note that we report MORL performance only as an oracle baseline, illustrating the maximum alignment achievable.

Prompt datasets: We use two benchmark datasets in our experiments. (i) We first select the color subset from DrawBench (Saharia et al., 2022b), comprising 25 prompts out of the full 183 prompts across 11 categories. RL training can reliably converge at this small-scale setup, which aligns with our theoretical assumption that RL converges to the closed-form solution of eq. (3), while our DB algorithm is interpolating between those optimal solutions under individual reward functions. For evaluation, we generate a test set of 1,000 prompts using a pipeline similar to GenEval with random color-object combinations. The candidate lists of colors and objects are generated by GPT-4 (Achiam et al., 2023) to be semantically similar to the training set (implementation details and full list in our code). (ii) We also validate performance of DB on the GenEval dataset (Kirstain et al., 2023), which contains 550 prompts across six compositional tasks: single objects, two objects, counting, colors, spatial positions, and color attribution. An additional 700 test prompts are generated using the official GenEval prompt generation script.

Training and evaluation details: We use Stable Diffusion v1.5 (SDv1.5) (Rombach et al., 2022) as the base model for our experiments, which is a text-to-image model capable of generating high-resolution images. We use the DPOK algorithm (Fan et al., 2023) for RL fine-tuning. For the experimental results given in the main paper, we use the 1000 test prompts. Details of the implementation, including training configurations and hyperparameters, are given in appendix B.3.

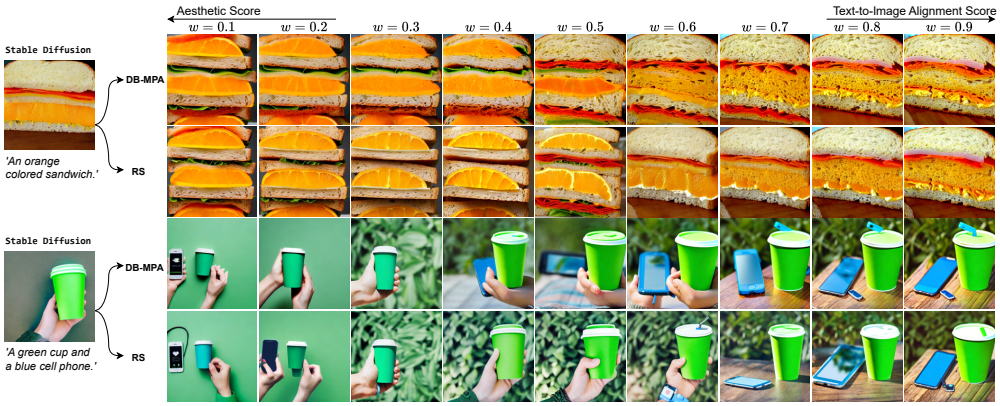

Figure 4: Illustration of the smooth control of DB-MPA to generate images aligned with $r(w)$ for any $w \in [0, 1]$. DB-MPA generates images that are better aligned with both rewards, especially for $w \in [0.4, 0.8]$. RS generates images with wrong interpretation objects (orange) or missing objects (cellphone).

5.1 DB-MPA Algoritm Results

Table 1: Quantitative comparison of DB-MPA and baseline methods

		SD		MORL		DB-MPA		DB-MPA-LS		RS		CoDe		RGG	
		r_1	r_2	r_1	r_2	r_1	r_2	r_1	r_2	r_1	r_2	r_1	r_2	r_1	r_2
Reward (↑)	w=0.0	-0.22	-0.14	-0.19	**0.47**	-0.19	**0.47**	-0.19	**0.47**	-0.19	**0.47**	**-0.02**	0.01	-0.16	0.42
	w=0.2	-0.22	-0.14	**0.24**	**0.38**	0.05	**0.38**	0.07	0.36	-0.20	0.23	0.16	0.00	-0.25	0.32
	w=0.5	-0.22	-0.14	**0.34**	0.14	0.27	**0.21**	0.31	0.14	-0.12	-0.04	0.30	-0.04	-0.08	0.14
	w=0.8	-0.22	-0.14	**0.43**	-0.11	0.36	**-0.01**	0.37	-0.04	0.21	-0.14	0.41	-0.10	0.21	-0.04
	w=1.0	-0.22	-0.14	**0.41**	-0.17	**0.41**	-0.17	**0.41**	-0.17	**0.41**	-0.17	0.40	**-0.15**	0.34	-0.18
Inference Time (↓ sec/img)		**5.46**		**5.46**		11.11		5.64		**5.46**		185.26		121.58	

We first consider two reward functions ($m = 2$), with r_1 as ImageReward (Xu et al., 2024), which measures text-image alignment, and r_2 as VILA (Kirstain et al., 2023), which measures aesthetics. During the inference time, the user specifies a preference weight $w \in [0, 1]$ to obtain data samples aligned to the reward $wr_1 + (1 - w)r_2$. We fix $\alpha = 0.1$ for these experiments, where α is the KL weight.

In fig. 2(b), we present the Pareto-front of DB-MPA against baseline algorithms under the *Short-DrawBench* setting, evaluated on the test prompts. For DB-MPA and RS, we evaluate the performance for $w \in \{0.1, \ldots, 0.9\}$. For other baselines, we evaluate their performance for $w \in \{0.2, 0.5, 0.8\}$ due to their high inference cost. Our DB-MPA algorithm consistently outperforms the baseline in all these experiments and achieves a Pareto-front very close to that of MORL, which represents the theoretical optimum obtainable by RL fine-tuning. We further evaluate the lightweight variant DB-MPA-LS, which achieves nearly identical Pareto performance while matching the inference speed of standard Stable Diffusion. As shown in fig. 11, the outputs of DB-MPA and DB-MPA-LS are also visually close. In table 1, we provide a quantitative comparison of this Pareto-front result. If we take the weighted reward $r(w)$ as a metric of comparison, for $w = 0.5$, DB-MPA (0.42) has close performance to DB-MPA-LS 0.39 and outperforms RS, CoDe, and RGG by **3.92**×, **1.95**×, and **1.33**×, respectively. table 1 also shows the inference time comparison. DB-MPA uses two fine-tuned models, making its inference time about twice that of Stable Diffusion. CoDe and RGG, though single-model methods, incur far higher costs due to multi-particle sampling and gradient steps. The lightweight DB-MPA-LS matches DB-MPA's performance while running at nearly the same speed as Stable Diffusion.

We further scale DB-MPA to the GenEval benchmark by fine-tuning models on all 550 prompts. Evaluation on the 700 held-out GenEval test prompts (table 4 and its corresponding Pareto boundary in fig. 5) shows that both DB-MPA and DB-MPA-LS consistently dominate the baselines across all preference weights.

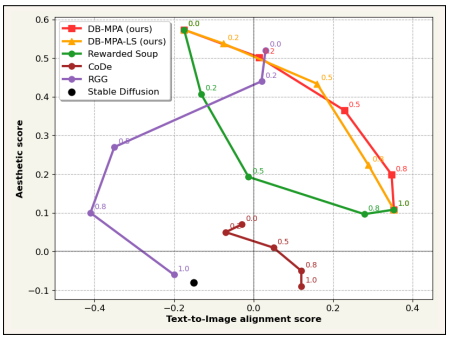

Figure 5: Pareto-front comparison of DB-MPA and DB-MPA-LS algorithm with other baselines, evaluated on GenEval test promt set.

fig. 4 illustrates the smooth control of DB-MPA in generating images aligned with $r(w)$ for any $w \in [0, 1]$. We use RS as the primary baseline due to the high inference cost of other methods. DB-MPA consistently produces images better aligned with both r_1 and r_2, particularly for $w \in [0.4, 0.8]$. Additional results in appendix C.8 and appendix C.9 further confirm that DB-MPA generates images of higher quality than the baseline and comparable to those from MORL.

We further examine a challenging case of conflicting rewards by introducing the *JPEG compressibility* reward, which favors smooth, low-detail images and directly opposes the VILA aesthetic reward that emphasizes fine-grained visual quality. As shown in appendix C.3, DB-MPA maintains superior performance even under this adversarial setting. We also extend our study to the three-reward case ($m = 3$) by incorporating *PickScore* (Kirstain et al., 2023), which measures human preference alignment. The corresponding results, provided in appendix C.5, validate the generalizability of our method to multi-reward settings while consistently achieving superior performance.

5.2 DB-KLA Algorithm Experiments

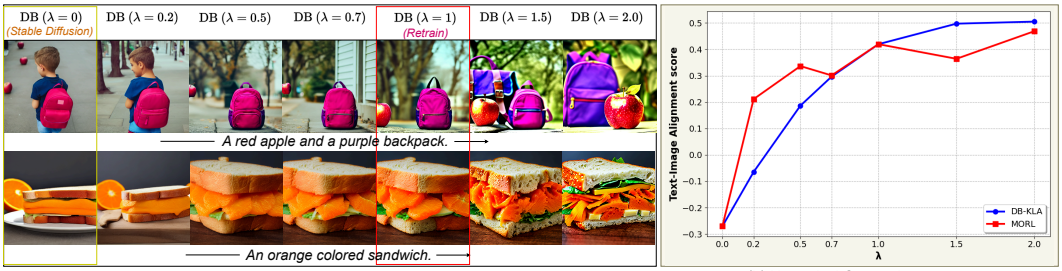

(a) degree of control of DB-KLA (b) Numerical Comparison

Figure 6: (a) Images generated by DB-KLA for different values of λ. We consider SDv1.5 as $\lambda = 0$ (infinite regularization weight), and as we increase λ, the aligned model moves further away from SDv1.5. These examples demonstrate that DB-KLA can smoothly control the level of text-to-image alignment by selecting different λ, without any additional fine-tuning. (b) The quantitative comparison of DB-KLA and λ-specific RL fine-tuned models among the test prompt set. Result for the train set is given in appendix D.

For the DB-KLA algorithm, we first fine-tune the baseline SVv1.5 model with the ImageReward and KL regularization weight $\alpha = 0.1$, using the *Short-DrawBench* prompts for fine-tuning and evaluation. In fig. 3(c), we show that *even without any additional fine-tuning, the images generated by DB-KLA are similar to those of λ-specific RL fine-tuned models*. In fig. 6(a), we illustrate that *DB-KLA enables smooth and continuous control over alignment strength via the rescaling factor λ*. Additional experiment results are given in appendix D. In fig. 6(b), we can observe that the average reward obtained by DB-KLA closely follows that of the MORL retrained model. As observed in fig. 6(a), in scenarios where the retrained model fails to fully align, DB-KLA with a stronger alignment setting ($\lambda > 1$) can generate more semantically accurate outputs, such as correcting object colors or preserving scene elements. This highlights its potential as a diagnostic tool for understanding and mitigating under- or over-optimization in reward-guided diffusion finetuning.

6 Conclusions

We introduced Diffusion Blend, a framework for inference-time multi-preference alignment in diffusion models that supports user-specified reward combinations and regularization strengths without requiring additional fine-tuning. Our proposed algorithms, DB-MPA, DB-MPA-LS, and DB-KLA, consistently outperform existing baselines and closely match the performance of individually fine-tuned models. Notably, DB-MPA-LS eliminates the linear scaling of inference time that plagues traditional inference time realignment methods, enabling efficient multi-preference alignment at scale.

REFERENCES

Josh Achiam, Steven Adler, Sandhini Agarwal, Lama Ahmad, Ilge Akkaya, Florencia Leoni Aleman, Diogo Almeida, Janko Altenschmidt, Sam Altman, Shyamal Anadkat, et al. Gpt-4 technical report. *arXiv preprint arXiv:2303.08774*, 2023.

Brian DO Anderson. Reverse-time diffusion equation models. *Stochastic Processes and their Applications*, 12(3):313–326, 1982.

Arpit Bansal, Hong-Min Chu, Avi Schwarzschild, Soumyadip Sengupta, Micah Goldblum, Jonas Geiping, and Tom Goldstein. Universal guidance for diffusion models. In *Proceedings of the IEEE/CVF Conference on Computer Vision and Pattern Recognition*, pages 843–852, 2023.

Ahmad Beirami, Alekh Agarwal, Jonathan Berant, Alexander D'Amour, Jacob Eisenstein, Chirag Nagpal, and Ananda Theertha Suresh. Theoretical guarantees on the best-of-n alignment policy. *arXiv preprint arXiv:2401.01879*, 2024.

Kevin Black, Michael Janner, Yilun Du, Ilya Kostrikov, and Sergey Levine. Training diffusion models with reinforcement learning. In *The Twelfth International Conference on Learning Representations*, 2024.

George Casella and Roger Berger. *Statistical inference*. CRC press, 2024.

Hyungjin Chung, Jeongsol Kim, Michael Thompson McCann, Marc Louis Klasky, and Jong Chul Ye. Diffusion posterior sampling for general noisy inverse problems. In *International Conference on Learning Representations, ICLR*, 2023.

Kevin Clark, Paul Vicol, Kevin Swersky, and David J. Fleet. Directly fine-tuning diffusion models on differentiable rewards. In *International Conference on Learning Representations, ICLR*, 2024.

Bradley Efron. Tweedie's formula and selection bias. *Journal of the American Statistical Association*, 106(496):1602–1614, 2011.

Ying Fan, Olivia Watkins, Yuqing Du, Hao Liu, Moonkyung Ryu, Craig Boutilier, Pieter Abbeel, Mohammad Ghavamzadeh, Kangwook Lee, and Kimin Lee. Dpok: Reinforcement learning for fine-tuning text-to-image diffusion models. *Advances in Neural Information Processing Systems*, 36:79858–79885, 2023.

Lin Gui, Cristina Garbacea, and Victor Veitch. Bonbon alignment for large language models and the sweetness of best-of-n sampling. In *Advances in Neural Information Processing Systems 38: Annual Conference on Neural Information Processing Systems*, 2024.

Yiju Guo, Ganqu Cui, Lifan Yuan, Ning Ding, Zexu Sun, Bowen Sun, Huimin Chen, Ruobing Xie, Jie Zhou, Yankai Lin, et al. Controllable preference optimization: Toward controllable multi-objective alignment. In *Proceedings of the 2024 Conference on Empirical Methods in Natural Language Processing*, pages 1437–1454, 2024.

Xu Han, Caihua Shan, Yifei Shen, Can Xu, Han Yang, Xiang Li, and Dongsheng Li. Training-free multi-objective diffusion model for 3d molecule generation. In *The Twelfth International Conference on Learning Representations*, 2023.

Yaru Hao, Zewen Chi, Li Dong, and Furu Wei. Optimizing prompts for text-to-image generation. *Advances in Neural Information Processing Systems*, 36:66923–66939, 2023.

Yutong He, Naoki Murata, Chieh-Hsin Lai, Yuhta Takida, Toshimitsu Uesaka, Dongjun Kim, Wei-Hsiang Liao, Yuki Mitsufuji, J. Zico Kolter, Ruslan Salakhutdinov, and Stefano Ermon. Manifold preserving guided diffusion. In *International Conference on Learning Representations, ICLR*, 2024.

Jonathan Ho, Ajay Jain, and Pieter Abbeel. Denoising diffusion probabilistic models. In *Advances in Neural Information Processing Systems (NeurIPS)*, volume 33, pages 6840–6851, 2020.

Joel Jang, Seungone Kim, Bill Yuchen Lin, Yizhong Wang, Jack Hessel, Luke Zettlemoyer, Hannaneh Hajishirzi, Yejin Choi, and Prithviraj Ammanabrolu. Personalized soups: Personalized large language model alignment via post-hoc parameter merging. *arXiv preprint arXiv:2310.11564*, 2023.

Junjie Ke, Keren Ye, Jiahui Yu, Yonghui Wu, Peyman Milanfar, and Feng Yang. Vila: Learning image aesthetics from user comments with vision-language pretraining. In *Proceedings of the IEEE/CVF Conference on Computer Vision and Pattern Recognition*, pages 10041–10051, 2023.

Sunwoo Kim, Minkyu Kim, and Dongmin Park. Test-time alignment of diffusion models without reward over-optimization. In *The Thirteenth International Conference on Learning Representations*, 2025.

Yuval Kirstain, Adam Polyak, Uriel Singer, Shahbuland Matiana, Joe Penna, and Omer Levy. Pick-a-pic: An open dataset of user preferences for text-to-image generation. *Advances in Neural Information Processing Systems*, 36:36652–36663, 2023.

Kyungmin Lee, Xiaohang Li, Qifei Wang, Junfeng He, Junjie Ke, Ming-Hsuan Yang, Irfan Essa, Jinwoo Shin, Feng Yang, and Yinxiao Li. Calibrated multi-preference optimization for aligning diffusion models. *arXiv preprint arXiv:2502.02588*, 2025.

Seung Hyun Lee, Yinxiao Li, Junjie Ke, Innfarn Yoo, Han Zhang, Jiahui Yu, Qifei Wang, Fei Deng, Glenn Entis, Junfeng He, et al. Parrot: Pareto-optimal multi-reward reinforcement learning framework for text-to-image generation. In *European Conference on Computer Vision*, pages 462–478. Springer, 2024.

Xiner Li, Yulai Zhao, Chenyu Wang, Gabriele Scalia, Gokcen Eraslan, Surag Nair, Tommaso Biancalani, Shuiwang Ji, Aviv Regev, Sergey Levine, et al. Derivative-free guidance in continuous and discrete diffusion models with soft value-based decoding. *arXiv preprint arXiv:2408.08252*, 2024.

Tianlin Liu, Shangmin Guo, Leonardo Bianco, Daniele Calandriello, Quentin Berthet, Felipe Llinares-López, Jessica Hoffmann, Lucas Dixon, Michal Valko, and Mathieu Blondel. Decoding-time realignment of language models. In *International Conference on Machine Learning*, pages 31015–31031. PMLR, 2024.

Sidharth Mudgal, Jong Lee, Harish Ganapathy, Yaguang Li, Tao Wang, Yanping Huang, Zhifeng Chen, Heng-Tze Cheng, Michael Collins, Trevor Strohman, et al. Controlled decoding from language models. In *International Conference on Machine Learning*, pages 36486–36503. PMLR, 2024.

Long Ouyang, Jeffrey Wu, Xu Jiang, Diogo Almeida, Carroll Wainwright, Pamela Mishkin, Chong Zhang, Sandhini Agarwal, Katarina Slama, Alex Ray, et al. Training language models to follow instructions with human feedback. *Advances in neural information processing systems*, 35: 27730–27744, 2022.

Rafael Rafailov, Archit Sharma, Eric Mitchell, Christopher D Manning, Stefano Ermon, and Chelsea Finn. Direct preference optimization: Your language model is secretly a reward model. *Advances in Neural Information Processing Systems*, 36:53728–53741, 2023.

Alexandre Rame, Guillaume Couairon, Corentin Dancette, Jean-Baptiste Gaya, Mustafa Shukor, Laure Soulier, and Matthieu Cord. Rewarded soups: towards pareto-optimal alignment by interpolating weights fine-tuned on diverse rewards. *Advances in Neural Information Processing Systems*, 36:71095–71134, 2023.

Aditya Ramesh, Prafulla Dhariwal, Alex Nichol, Casey Chu, and Mark Chen. Hierarchical text-conditional image generation with clip latents. *arXiv preprint arXiv:2204.06125*, 1(2):3, 2022.

Diederik M Roijers, Peter Vamplew, Shimon Whiteson, and Richard Dazeley. A survey of multi-objective sequential decision-making. *Journal of Artificial Intelligence Research*, 48:67–113, 2013.

Robin Rombach, Andreas Blattmann, Dominik Lorenz, Patrick Esser, and Björn Ommer. High-resolution image synthesis with latent diffusion models. In *Proceedings of the IEEE/CVF Conference on Computer Vision and Pattern Recognition (CVPR)*, pages 10684–10695, June 2022.

Litu Rout, Negin Raoof, Giannis Daras, Constantine Caramanis, Alex Dimakis, and Sanjay Shakkottai. Solving linear inverse problems provably via posterior sampling with latent diffusion models. In *Advances in Neural Information Processing Systems 36: Annual Conference on Neural Information Processing Systems*, 2023.

Litu Rout, Yujia Chen, Abhishek Kumar, Constantine Caramanis, Sanjay Shakkottai, and Wen-Sheng Chu. Beyond first-order tweedie: Solving inverse problems using latent diffusion. In *Proceedings of the IEEE/CVF Conference on Computer Vision and Pattern Recognition*, pages 9472–9481, 2024.

Chitwan Saharia, William Chan, Saurabh Saxena, Lala Li, Jay Whang, Emily L Denton, Kamyar Ghasemipour, Raphael Gontijo Lopes, Burcu Karagol Ayan, Tim Salimans, et al. Photorealistic text-to-image diffusion models with deep language understanding. *Advances in neural information processing systems*, 35:36479–36494, 2022a.

Chitwan Saharia, William Chan, Saurabh Saxena, Lala Li, Jay Whang, Emily L Denton, Kamyar Ghasemipour, Raphael Gontijo Lopes, Burcu Karagol Ayan, Tim Salimans, et al. Photorealistic text-to-image diffusion models with deep language understanding. *Advances in Neural Information Processing Systems*, 35:36479–36494, 2022b.

Ruizhe Shi, Yifang Chen, Yushi Hu, Alisa Liu, Hanna Hajishirzi, Noah A Smith, and Simon S Du. Decoding-time language model alignment with multiple objectives. *Advances in Neural Information Processing Systems*, 37:48875–48920, 2024.

Anuj Singh, Sayak Mukherjee, Ahmad Beirami, and Hadi Jamali-Rad. Code: Blockwise control for denoising diffusion models. *arXiv preprint arXiv:2502.00968*, 2025.

Raghav Singhal, Zachary Horvitz, Ryan Teehan, Mengye Ren, Zhou Yu, Kathleen McKeown, and Rajesh Ranganath. A general framework for inference-time scaling and steering of diffusion models. *arXiv preprint arXiv:2501.06848*, 2025.

Jiaming Song, Chenlin Meng, and Stefano Ermon. Denoising diffusion implicit models. *arXiv preprint arXiv:2010.02502*, 2020.

Jiaming Song, Qinsheng Zhang, Hongxu Yin, Morteza Mardani, Ming-Yu Liu, Jan Kautz, Yongxin Chen, and Arash Vahdat. Loss-guided diffusion models for plug-and-play controllable generation. In *International Conference on Machine Learning*, pages 32483–32498. PMLR, 2023.

Yang Song, Jascha Sohl-Dickstein, Diederik P Kingma, Abhishek Kumar, Stefano Ermon, and Ben Poole. Score-based generative modeling through stochastic differential equations. In *International Conference on Learning Representations (ICLR)*, 2021.

Masatoshi Uehara, Yulai Zhao, Tommaso Biancalani, and Sergey Levine. Understanding reinforcement learning-based fine-tuning of diffusion models: A tutorial and review. *arXiv preprint arXiv:2407.13734*, 2024a.

Masatoshi Uehara, Yulai Zhao, Kevin Black, Ehsan Hajiramezanali, Gabriele Scalia, Nathaniel Lee Diamant, Alex M Tseng, Tommaso Biancalani, and Sergey Levine. Fine-tuning of continuous-time diffusion models as entropy-regularized control. *arXiv preprint arXiv:2402.15194*, 2024b.

Haoxiang Wang, Yong Lin, Wei Xiong, Rui Yang, Shizhe Diao, Shuang Qiu, Han Zhao, and Tong Zhang. Arithmetic control of llms for diverse user preferences: Directional preference alignment with multi-objective rewards. In *Proceedings of the 62nd Annual Meeting of the Association for Computational Linguistics (Volume 1: Long Papers)*, pages 8642–8655, 2024a.

Kaiwen Wang, Rahul Kidambi, Ryan Sullivan, Alekh Agarwal, Christoph Dann, Andrea Michi, Marco Gelmi, Yunxuan Li, Raghav Gupta, Kumar Dubey, et al. Conditional language policy: A general framework for steerable multi-objective finetuning. In *Findings of the Association for Computational Linguistics: EMNLP 2024*, pages 2153–2186, 2024b.

Zeqiu Wu, Yushi Hu, Weijia Shi, Nouha Dziri, Alane Suhr, Prithviraj Ammanabrolu, Noah A Smith, Mari Ostendorf, and Hannaneh Hajishirzi. Fine-grained human feedback gives better rewards for language model training. *Advances in Neural Information Processing Systems*, 36:59008–59033, 2023.

Jiazheng Xu, Xiao Liu, Yuchen Wu, Yuxuan Tong, Qinkai Li, Ming Ding, Jie Tang, and Yuxiao Dong. Imagereward: Learning and evaluating human preferences for text-to-image generation. *Advances in Neural Information Processing Systems*, 36, 2024.

Rui Yang, Xiaoman Pan, Feng Luo, Shuang Qiu, Han Zhong, Dong Yu, and Jianshu Chen. Rewards-in-context: Multi-objective alignment of foundation models with dynamic preference adjustment. In *International Conference on Machine Learning*, 2024.

Runzhe Yang, Xingyuan Sun, and Karthik Narasimhan. A generalized algorithm for multi-objective reinforcement learning and policy adaptation. *Advances in neural information processing systems*, 32, 2019.

Haotian Ye, Haowei Lin, Jiaqi Han, Minkai Xu, Sheng Liu, Yitao Liang, Jianzhu Ma, James Y Zou, and Stefano Ermon. Tfg: Unified training-free guidance for diffusion models. *Advances in Neural Information Processing Systems*, 37:22370–22417, 2024.

Jiwen Yu, Yinhuai Wang, Chen Zhao, Bernard Ghanem, and Jian Zhang. Freedom: Training-free energy-guided conditional diffusion model. In *Proceedings of the IEEE/CVF International Conference on Computer Vision*, pages 23174–23184, 2023.

Ming Zhong, Yelong Shen, Shuohang Wang, Yadong Lu, Yizhu Jiao, Siru Ouyang, Donghan Yu, Jiawei Han, and Weizhu Chen. Multi-lora composition for image generation. *Transactions on Machine Learning Research*, 2024, 2024a.

Yifan Zhong, Chengdong Ma, Xiaoyuan Zhang, Ziran Yang, Haojun Chen, Qingfu Zhang, Siyuan Qi, and Yaodong Yang. Panacea: Pareto alignment via preference adaptation for llms. *Advances in Neural Information Processing Systems*, 37:75522–75558, 2024b.

Ruida Zhou, Tao Liu, Dileep Kalathil, PR Kumar, and Chao Tian. Anchor-changing regularized natural policy gradient for multi-objective reinforcement learning. *Advances in neural information processing systems*, 35:13584–13596, 2022.

Xiandong Zou, Mingzhu Shen, Christos-Savvas Bouganis, and Yiren Zhao. Cached multi-lora composition for multi-concept image generation. *arXiv preprint arXiv:2502.04923*, 2025.

A TECHNICAL PROOFS

In this section, we provide the theoretical details referenced in Section 4. We begin by analyzing the solution to eq. (3), followed by a discussion of the Jensen gap approximation error introduced by interchanging the expectation operator $\mathbb{E}[\cdot]$ and the exponential function $\exp(\cdot)$. We then describe how to approximate a general function $f^{(r(w),\alpha(\lambda))}$ under the Jensen gap approximation. Finally, we provide an analysis for the sampling-based approximation algorithm based on SDE theory showing its equivalent marginal distribution.

A.1 PROOF OF PROPOSITION 1

Proof of Proposition 1. By definition, $p_t^{\mathrm{pre}}(x) = \int_y p_0^{\mathrm{pre}}(y)p_{\epsilon_t}(x-y)\ \mathrm{d}y, p_t^{\mathrm{tar}}(x) = \int_y p_0^{\mathrm{tar}}(y)p_{\epsilon_t}(x-y)\ \mathrm{d}y$. We also have, $p_{0|t}^{\mathrm{pre}}(x_0|x_t) = \frac{p_{0,t}^{\mathrm{pre}}(x_0,x_t)}{p_t^{\mathrm{pre}}(x_t)} = \frac{p_0^{\mathrm{pre}}(x_0)p_{\epsilon_t}(x_t-x_0)}{p_t^{\mathrm{pre}}(x_t)}$. Now, with an appropriate normalization constant C,

$$
\begin{aligned}
p_t^{\mathrm{tar}}(x) &= \int_y p_0^{\mathrm{tar}}(y)p_{\epsilon_t}(x-y)\ \mathrm{d}y = C\int_y p_0^{\mathrm{pre}}(y)\exp\left(\frac{r(y)}{\alpha}\right)p_{\epsilon_t}(x-y)\ \mathrm{d}y \\
&= Cp_t^{\mathrm{pre}}(x)\int_y \exp\left(\frac{r(y)}{\alpha}\right)\frac{p_0^{\mathrm{pre}}(y)p_{\epsilon_t}(x-y)}{p_t^{\mathrm{pre}}(x)}\ \mathrm{d}y = Cp_t^{\mathrm{pre}}(x)\int_y \exp\left(\frac{r(y)}{\alpha}\right)p_{0|t}^{\mathrm{pre}}(y|x)\ \mathrm{d}y \\
&= Cp_t^{\mathrm{pre}}(x)\mathbb{E}_{x_0\sim p_{0|t}^{\mathrm{pre}}(\cdot|x)}\left[\exp\left(\frac{r(x_0)}{\alpha}\right)\right].
\end{aligned}
$$

From this, we get,

$$
\nabla_x \log p_t^{\mathrm{tar}}(x) = \nabla_x \log p_t^{\mathrm{tar}}(x) + \nabla_x \log \mathbb{E}_{x_0\sim p_{0|t}^{\mathrm{pre}}(\cdot|x)}\left[\exp\left(\frac{r(x_0)}{\alpha}\right)\right]. \tag{11}
$$

The result now follows from the definition of $f^{(r,\alpha)}(x_t) = -\frac{1}{2}\beta(t)x_t - \beta(t)\nabla_{x_t}\log p_t^{\mathrm{tar}}(x_t)$ and $f^{\mathrm{pre}}(x_t) = -\frac{1}{2}\beta(t)x_t - \beta(t)\nabla_{x_t}\log p_t^{\mathrm{pre}}(x_t)$. □

We also present a more general formulation of proposition 1 to offer a clearer understanding.

Proposition 3 (General statement of proposition 1)**.** *Let X be a random variable distributed according to $p_0(x)$, Y be a random variable distributed as $q_0(y) = Cp_0(y)\exp(r(y)/\alpha)$, and Z be an independent noise. If the probability density of $X+Z$ is p_t, then the probability density of $Y+Z$ is $q_t(x) = Cp_t(x)\mathbb{E}[\exp(\frac{r(X)}{\alpha})|X+Z=x]$. The score of $Y+Z$ is given by $\nabla_x \log \mathbb{E}[\exp(\frac{r(X)}{\alpha})|X+Z=x] + \nabla \log p_t(x)$.*

Proof. Note $X+Z$ is distributed w.r.t. the probability density:

$$
p_t(x) = \int p_0(y)p_Z(x-y)dy.
$$

Density of $Y+Z$ is:

$$
\begin{aligned}
& q_t(x) \\
=& \int q_0(y)p_Z(x-y)dy \\
=& C\int p_0(y)\exp(\frac{r(y)}{\alpha})p_Z(x-y)dy \\
=& Cp_t(x)\int \exp(\frac{r(y)}{\alpha})\frac{p_0(y)p_Z(x-y)}{\int p_0(s)p_Z(x-s)ds}dy \\
=& Cp_t(x)\int \exp(\frac{r(y)}{\alpha})p_{X|X+Z=x}(X=y)dy \\
=& Cp_t(x)\mathbb{E}\Big[\exp(\frac{r(X)}{\alpha})\Big|X+Z=x\Big].
\end{aligned}
$$

□

Remark 3. Consider the variance-exploding forward process proposed by Song et al. (2021), i.e. $X_t = X_0 + \sqrt{\bar{\alpha}_t} Z$ with $Z \sim \mathcal{N}(0, I)$. proposition 3 implies that for two different initial distributions $X \sim p_0$ and $Y \sim q_0 \propto p_0 \exp(r/\alpha)$, both following the same noise-exploding forward process, the marginal probability density $q_t(y)$ of $Y_t = Y_0 + \sqrt{\bar{\alpha}_t} Z$ is equal to the product of the density of X_t and a posterior mean term $\mathbb{E}[\exp(r(X_0)/\alpha) \mid X_t = y]$. Recall that the reverse process involves adding an extra score term $\nabla_x \log p_t(x)$ into the drift. proposition 3 suggests that approximating $p_0^{\text{pre}} \exp(r/\alpha)$ in the reverse process can be achieved by replacing the original score $\nabla \log p_t(x)$ in X_t, with a shifted score $\nabla_x \log p_t(x) + \nabla_x \log \mathbb{E}[\exp(r(X_0)/\alpha) \mid X_t = x]$.

The same analysis applies to the variance-preserving forward process used in DDPM (Ho et al., 2020), defined as $X_t = \sqrt{\bar{\alpha}_t} X_0 + \sqrt{1 - \bar{\alpha}_t} Z$ with $Z \sim \mathcal{N}(0, I)$. In this case, the same conclusion follows by replacing the random variable X in proposition 3 with $\sqrt{\bar{\alpha}_t} X_0$.

A.2 Approximation Error Upper bound for eq. (8)

Lemma 2. *Decompose the reward function into two parts*

$$\frac{r(x_0^{\text{pre}})}{\alpha} = \tilde{r}(x_t^{\text{pre}}, t) + \eta(\omega, x_t^{\text{pre}}, t)$$

where $\tilde{r}(x_t^{\text{pre}}, t) = \mathbb{E}[\frac{r(x_0^{\text{pre}})}{\alpha} | x_t^{\text{pre}}]$ *only depends on* x_t^{pre} *and* $\eta(\omega, x_t^{\text{pre}}, t) = \frac{r(x_0^{\text{pre}})}{\alpha} - \tilde{r}(x_t^{\text{pre}}, t)$ *contains randomness* ω *induced from the noise injection process. Let* $p_{R|t}$ *denote the conditional distribution of random variable* $R := r(x_0^{\text{pre}})/\alpha$ *given* x_t^{pre}*. Then,*
$\|\nabla_x \log \mathbb{E}[\exp(r(x_0^{\text{pre}})/\alpha) | x_t^{\text{pre}} = x] - \nabla_x \mathbb{E}[r(x_0^{\text{pre}})/\alpha | x_t^{\text{pre}} = x]\| \le L_{t,1}(x) \times L_{t,2}(x) + L_{t,3}(x)$, *where*

$$L_{t,1}(x) = \sqrt{\mathbb{E}[\|\nabla_x \eta(\omega, x_t^{\text{pre}}, t)\|_2^2 | x_t^{\text{pre}} = x]},$$
$$L_{t,2}(x) = \frac{\sqrt{\text{Var}(\exp(r(x_0^{\text{pre}})/\alpha) | x_t^{\text{pre}} = x)}}{\mathbb{E}[\exp(r(x_0^{\text{pre}})/\alpha) | x_t^{\text{pre}} = x]},$$
$$L_{t,3}(x) = (1 + \frac{1}{\alpha}) \sup_r \|\nabla_x \log p_{R|t}(r | x_t^{\text{pre}} = x) + \nabla_r \log p_{R|t}(r | x_t^{\text{pre}} = x)\|.$$

Proof. To shorten the notation, we denote random variable $R := r(x_0^{\text{pre}})/\alpha$ and constant $C_R = \max_x |r(x)/\alpha| = \frac{1}{\alpha}$. Let $p_{R|t}$ be the conditional probability of R given x_t.

We first make one assumption about the boundary condition that the conditional probability density decreases exponentially fast $\lim_{r \to \pm\infty} r \cdot p_{R|t}(r|x) = 0$, and $\lim_{r \to \pm\infty} e^r \cdot p_{R|t}(r|x) = 0$. It is known that sub-Gaussian distributions satisfy those assumptions with an exponentially decreasing tail $p(x) \le C e^{-|x|^\alpha}$ for large enough x. Remember that in our experimental setting, all reward models output in a bounded range $[-2, 2]$ and α is a fixed real number. Therefore, for the bounded random variable R, it belongs to the sub-Gaussian distribution and satisfies our boundary assumption.

Let $F(x) = \mathbb{E}[\exp(R) | x_t^{\text{pre}} = x]$ and $g(x) = \mathbb{E}[R | x_t^{\text{pre}} = x]$, then

$$\begin{aligned}
&\nabla_x \log F(x) - \nabla_x g(x) = \frac{\nabla_x F(x)}{F(x)} - \nabla_x g(x) \\
=&\frac{\int \nabla_x \exp(r) \cdot p_{R|t}(r|x) dr + \int \exp(r) \nabla_x p_{R|t}(r|x) dr}{F(x)} \\
&- \Big(\int \nabla_x r \cdot p_{R|t}(r|x) + r \nabla_x p_{R|t}(r|x) dr \Big) \\
=&\frac{\mathbb{E}[\nabla_{x_t^{\text{pre}}} \exp(R) | x_t^{\text{pre}} = x]}{F(x)} - \mathbb{E}[\nabla_{x_t^{\text{pre}}} R | x_t^{\text{pre}} = x] \\
&+ \Big(\frac{\int \exp(r) \nabla_x p_{R|t}(r|x) dr}{F(x)} - \int r \nabla_x p_{R|t}(r|x) dr \Big) \\
=&\underbrace{\mathbb{E}\left[\left(\frac{\exp(R)}{F(x)} - 1 \right) \nabla_{x_t^{\text{pre}}} R \Big| x_t^{\text{pre}} = x \right]}_{I_1} + \underbrace{\Big(\frac{\int \exp(r) \nabla_x p_{R|t}(r|x) dr}{F(x)} - \int r \nabla_x p_{R|t}(r|x) dr \Big)}_{I_2}.
\end{aligned}$$

We first bound the first term I_1. Decompose R into two parts $R = \tilde{r}(x_t^{\text{pre}}, t) + \eta(\omega, x_t^{\text{pre}}, t)$ where the first part $\tilde{r}(x_t^{\text{pre}}, t)$ only depends on x_t^{pre}. Note that $\mathbb{E}[\frac{\exp(R)}{F(x)} - 1 | x_t^{\text{pre}} = x] = \mathbb{E}[\frac{\exp(R)}{\mathbb{E}[\exp(R)|x_t^{\text{pre}}=x]} - 1 | x_t^{\text{pre}} = x] = 0$.

$$
\begin{aligned}
\|I_1\| =& \left\| \mathbb{E}\left[\left(\frac{e^R}{F(x)} - 1 \right) \nabla_{x_t^{\text{pre}}} R \middle| x_t^{\text{pre}} = x \right] \right\| \\
=& \left\| \mathbb{E}\left[\left(\frac{e^R}{F(x)} - 1 \right) (\nabla_{x_t^{\text{pre}}} \tilde{r}(x_t^{\text{pre}}, t)) + \nabla_{x_t^{\text{pre}}} \eta(\omega, x_t^{\text{pre}}, t)) \middle| x_t^{\text{pre}} = x \right] \right\| \\
=& \left\| \mathbb{E}\left[\left(\frac{e^R}{F(x)} - 1 \right) \nabla_{x_t^{\text{pre}}} \eta(\omega, x_t^{\text{pre}}, t) \middle| x_t^{\text{pre}} = x \right] \right\| \\
\leq& \sqrt{\mathbb{E}\Big[\left(\frac{e^R}{F(x)} - 1 \right)^2 \Big| x_t^{\text{pre}} = x \Big]} \times \sqrt{\mathbb{E}\left[\|\nabla_{x_t^{\text{pre}}} \eta(\omega, x_t^{\text{pre}}, t)\|_2^2 \middle| x_t^{\text{pre}} = x \right]} \\
=& L_{t,2}(x) \times L_{t,1}(x).
\end{aligned}
$$

For the second term I_2, we note that $I_2 \equiv 0$ under the assumption proposed by Uehara et al. (2024b) that $R = f(x_t) + \epsilon$ can be decomposed to the summation of a function related to x_t and an independent noise ϵ, which is induced by the translation invariance of $p_{R|t}(r|x) = p_{\text{noise}}(r - x)$. Inspired by this observation, we define $\Delta_t := \nabla_x \log p_{R|t}(r|x) + \nabla_r \log p_{R|t}(r|x)$ to measure the shift from such a translation invariant family $\{p_{R|t} : \exists\, p_{noise},\ \text{s.t. } p_{R|t}(r|x) = p_{\text{noise}}(r - x)\}$.

$$
\begin{aligned}
I_2 =& \frac{\int \exp(r) p_{R|t}(r|x) \nabla_x \log p_{R|t}(r|x) dr}{F(x)} - \int r p_{R|t}(r|x) \nabla_x \log p_{R|t}(r|x) dr \\
=& \frac{\int \exp(r) p_{R|t}(r|x) (\Delta_t - \nabla_r \log p_{R|t}(r|x)) dr}{F(x)} - \int r p_{R|t}(r|x) (\Delta_t - \nabla_r \log p_{R|t}(r|x)) dr \\
=& \mathbb{E}_{p'}[\Delta_t | x_t^{\text{pre}} = x] - \mathbb{E}[r \Delta_t | x_t^{\text{pre}} = x] \\
& - \Big(\underbrace{\frac{\int \exp(r) p_{R|t}(r|x) \nabla_r \log p_{R|t}(r|x) dr}{F(x)}}_{I_F} - \underbrace{\int r p_{R|t}(r|x) \nabla_r \log p_{R|t}(r|x) dr}_{I_g} \Big),
\end{aligned}
$$

where $p'(r|x) = \frac{\exp(r) p_{R|t}(r|x)}{F(x)}$ is the reweighted probability. Under the boundary condition, we can show that $I_F = I_g = -1$ as

$$
\begin{aligned}
I_g =& \int r \nabla_r p_{R|t}(r|x) dr = \int \nabla_r (r p_{R|t}(r|x)) dr - \int p_{R|t}(r|x) dr \\
=& r p_{R|t}(r|x) \Big|_{r=-\infty}^{r=+\infty} - 1 = -1, \\
I_F =& \frac{\int \exp(r) \nabla_r p_{R|t}(r|x) dr}{F(x)} = \frac{\int \nabla_r \Big(\exp(r) p_{R|t}(r|x) \Big) dr - \int \exp(r) p_{R|t}(r|x) dr}{F(x)} \\
=& \frac{\int \nabla_r (\exp(r) p_{R|t}(r|x)) dr}{F(x)} - 1 = \frac{\Big(\exp(r) p_{R|t}(r|x) \Big) \Big|_{r=-\infty}^{r=+\infty}}{F(x)} - 1 = -1.
\end{aligned}
$$

Therefore, $\|I_2\| = \|\mathbb{E}_{p'}[\Delta_t | x_t^{\text{pre}} = x] - \mathbb{E}[r \Delta_t | x_t^{\text{pre}} = x]\| \leq (1 + C_R) \sup_{r,x} \|\Delta_t\| = L_{t,3}(x)$. □

Remark 4. In lemma 2, the term $L_{t,1}$ quantifies the local Lipschitz sensitivity of the stochastic component of R with respect to changes in x_t; $L_{t,2}$ denotes the conditional coefficient of variation (i.e., the ratio of standard deviation to mean) of R given x_t; and $L_{t,3}$ measures the deviation of the conditional distribution $p(x_0 \mid x_t)$ from a pure shift family. A shift family (or location family) refers to a class of conditional distributions where changing the conditioning variable results in a simple translation of the distribution without altering its shape, e.g., $P(X = x|Y = y) = P(X = x - y)$

(Casella and Berger, 2024). For a perfect shift family, we may write $L_{t,3} \equiv 0$. In diffusion models, as t gets closer to 0, $p^{\mathrm{pre}}_{0|t}(x_0|x_t)$ becomes more deterministic and concentrates around x_t, with variation of x_t reducing to a mean shift, resulting $L_{t,3}$ to get closer to 0. When the reward function is more predictable from the noisy image x_t or t becomes closer to 0, both $L_{t,1}$ and $L_{t,2}$ will be small. Note that $L_{t,2}$ and $L_{t,3}$ will increase when the regularization coefficient α becomes very small, suggesting that our algorithm might fail when we decrease α dramatically. We note that Uehara et al. (2024b) exchanges the order of $\mathbb{E}[\cdot]$ and $\exp(\cdot)$ under the assumption $r(x_0) = k(x_t) + \epsilon$, where ϵ is an independent noise term. This is consistent with our result, as it would be easy to derive $L_{t,1} \equiv L_{t,3} \equiv 0$ under their assumption.

A.3 Proof of Lemma 1

Proof of Lemma 1. By leveraging the linearity of expectation available in $\bar{u}^{(r(w),\alpha)}$, we get

$$\bar{u}^{(r(w),\alpha)}(x,t) = \nabla_x \mathbb{E}_{x_0 \sim p^{\mathrm{pre}}_{0|t}(\cdot|x)} \left[\left(\frac{\sum_{i=1}^m w_i r_i(x_0)}{\alpha} \right) \right] = \sum_{i=1}^m w_i \bar{u}^{(r_i,\alpha)}(x,t).$$

Using this, we get

$$\begin{aligned}
& f^{(r(w),\alpha)}(x_t,t) \\
=& f^{\mathrm{pre}}(x_t,t) - \beta(t) u^{(r(w),\alpha)}(x_t,t) = f^{\mathrm{pre}}(x_t,t) - \beta(t)\bar{u}^{(r(w),\alpha)}(x,t) - \beta(t)\Delta^{(r(w),\alpha)}(x,t) \\
=& f^{\mathrm{pre}}(x_t,t) - \beta(t)\sum_{i=1}^m w_i u^{(r_i,\alpha)}(x,t) + \beta(t)\left(\sum_{i=1}^m w_i \Delta^{(r_i,\alpha)}(x,t) - \Delta^{(r(w),\alpha)}(x,t) \right) \\
=& \sum_{i=1}^m w_i (f^{\mathrm{pre}}(x_t,t) - \beta(t) u^{(r_i,\alpha)}(x,t)) + \beta(t)\left(\sum_{i=1}^m w_i \Delta^{(r_i,\alpha)}(x,t) - \Delta^{(r(w),\alpha)}(x,t) \right) \\
=& \sum_{i=1}^m w_i f^{(r_i,\alpha)}(x_t,t) + \beta(t)\left(\sum_{i=1}^m w_i \Delta^{(r_i,\alpha)}(x,t) - \Delta^{(r(w),\alpha)}(x,t) \right).
\end{aligned}$$

Similarly, using the fact that $\bar{u}^{(r,\alpha(\lambda))}(x,t) = \lambda \bar{u}^{(r,\alpha)}(x,t)$, we get

$$\begin{aligned}
& f^{(r,\alpha(\lambda))}(x_t,t) \\
=& f^{\mathrm{pre}}(x_t,t) - \beta(t) u^{(r,\alpha(\lambda))}(x_t,t) = f^{\mathrm{pre}}(x_t,t) - \beta(t)\bar{u}^{(r,\alpha(\lambda))}(x,t) - \beta(t)\Delta^{(r,\alpha(\lambda))}(x,t) \\
=& f^{\mathrm{pre}}(x_t,t) - \beta(t)\lambda\bar{u}^{(r,\alpha)}(x,t) - \beta(t)\Delta^{(r,\alpha(\lambda))}(x,t) \\
=& \lambda(f^{\mathrm{pre}}(x_t,t) - \beta(t)\bar{u}^{(r,\alpha)}(x,t)) + (1-\lambda) f^{\mathrm{pre}}(x_t,t) - \beta(t)\Delta^{(r,\alpha(\lambda))}(x,t) \\
=& \lambda f^{(r,\alpha)}(x_t,t) + (1-\lambda) f^{\mathrm{pre}}(x_t,t) + \beta(t)\left(\lambda\Delta^{(r,\alpha)}(x,t) - \Delta^{(r,\alpha(\lambda))}(x,t) \right).
\end{aligned}$$

□

A.4 Proof of Proposition 2

Proof of Proposition 2. Denote $b(x) = af_1(x) + (1-a)f_2(x)$. For any function $\psi \in C^2(\mathbb{R}^d)$, Itô's formula gives:

$$\begin{aligned}
d\psi(X_t^1) &= \sigma(t)\nabla\psi(X_t^1)^T d\omega_t + [\nabla\psi(X_t^1)^T b(X_t^1) + \frac{\sigma^2(t)}{2} tr(\nabla^2\psi(X_t^1))]dt, \\
\frac{d}{dt}\mathbb{E}[\psi(X_t^1)] &= \int \sigma(t)\nabla\psi(X_t^1)^T d\omega_t + \mathbb{E}[\nabla\psi(X_t^1)^T b(X_t^1) + \frac{\sigma^2(t)}{2} tr(\nabla^2\psi(X_t^1))].
\end{aligned}$$

Note that $tr(\nabla^2\psi) = \Delta\psi$, and $\int \sigma(t)\nabla\psi(X_t^1)^T d\omega_t$ is a martingale with mean 0, therefore the first term in the RHS is 0. We got for SDE 1:

$$\frac{d}{dt}\mathbb{E}[\psi(X_t^1)] = \mathbb{E}[\nabla\psi(X_t^1)^T b(X_t^1) + \frac{\sigma^2(t)}{2}\Delta\psi(X_t^1)].$$

Move to the SDE 2. Similarly, we can derive:

$$\begin{aligned}\frac{d}{dt}\mathbb{E}[\psi(X_t^2)] &= \mathbb{E}[\nabla\psi(X_t^2)^T(Y_t f_1(X_t^2) + (1-Y_t)f_2(X_t^2)) + \frac{\sigma^2(t)}{2}\Delta\psi(X_t^2)] \\ &= \mathbb{E}[Y_t\nabla\psi(X_t^2)^T f_1(X_t^2] + \mathbb{E}[(1-Y_t)\nabla\psi(X_t^2)^T f_2(X_t^2)] + \mathbb{E}[\frac{\sigma^2(t)}{2}\Delta\psi(X_t^2)] \\ &= \mathbb{E}[Y_t]\mathbb{E}[\nabla\psi(X_t^2)^T f_1(X_t^2)] + \mathbb{E}[1-Y_t]\mathbb{E}[\nabla\psi(X_t^2)^T f_2(X_t^2)] + \mathbb{E}[\frac{\sigma^2(t)}{2}\Delta\psi(X_t^2)] \\ &= a\mathbb{E}[\nabla\psi(X_t^2)^T f_1(X_t^2)] + (1-a)\mathbb{E}[\nabla\psi(X_t^2)^T f_2(X_t^2)] + \mathbb{E}[\frac{\sigma^2(t)}{2}\Delta\psi(X_t^2)] \\ &= \mathbb{E}[\nabla\psi(X_t^2)b(X_t^2) + \frac{\sigma^2(t)}{2}\Delta\psi(X_t^2)],\end{aligned}$$

where the independence of $\{Y_t\}$ is applied.

Both $\{X_t^1\}$ and $\{X_t^2\}$ satisfy: $\frac{d}{dt}\mathbb{E}[\psi(X_t)] = \mathbb{E}[\nabla\psi(X_t)b(X_t) + \frac{\sigma^2(t)}{2}\Delta\psi(X_t)]$ with $X_0 \sim p_0$, for any $\psi \in C^2$. Denote p_t as the probability density of X_t, we got:

$$\begin{aligned}\frac{d}{dt}\int \psi(s)p_t(x)dx &= \int \left(\nabla\psi(x)b(x) + \frac{\sigma^2(t)}{2}\Delta\psi(x)\right)p_t(x)dx \\ \int \psi(s)\partial_t p_t(x)dx &= \int -\psi(x)\nabla\Big(b(x)p_t(x)\Big) + \frac{\sigma^2(t)}{2}\psi(x)\Delta p_t(x)dx,\end{aligned}$$

where the change of integral is used. Then we have:

$$\int \psi(s)\Big(\partial_t p_t(x)dx + \nabla(b(x)p_t(x)) - \frac{\sigma^2(t)}{2}\Delta p_t(x)\Big)dx = 0,\ \forall\psi \in C^2.$$

Therefore, both $p_{X_t^1}$ and $p_{X_t^2}$ are solutions of this PDE: $\partial_t p_t(x)dx + \nabla(b(x)p_t(x)) - \frac{\sigma^2(t)}{2}\Delta p_t(x) = 0$ with $p|_{t=0} = p_0$. Since the drift term b is Lipschitz continuous, this PDE has only one solution. Therefore, $p_{X_t^1} = p_{X_t^2}$. □

B Experimental Details

B.1 Baseline Algorithms

MORL: For MORL, we fine-tune the SDv1.5 base model using RL, following the same procedure as in Fan et al. (2023). In particular, we obtain separately fine-tuned models for $(r(w), \alpha(\lambda))$, for different values of w and λ. This is used as an oracle baseline for both DB-MPA and DB-KLA.

Rewarded Soup (RS): We use RS, introduced by Rame et al. (2023), as a baseline for the DB-MPA. We first RL fine-tune SDv1.5 separately for each reward each reward $(r_i)_{i=1}^m$ with a fixed α. So, starting from the pre-trained model parameter θ^{pre}, we obtained m RL fine-tuned models with parameters $(\theta_i^{\text{rl}})_{i=1}^m$. At inference time, given the preference w given by the user, we construct a new model with parameter $\theta^{\text{rs}}(w) = \sum_{i=1}^m w_i\theta_i^{\text{rl}}$, and generate images using this model. We only average the U-Net parameters from the fine-tuned models.

Reward Gradient Guidance (RGG): We follow the gradient guidance approach (Chung et al., 2023; Kim et al., 2025) where the diffusion process at each backward step is updated using the gradient of the reward function. The update rule is given by:

$$\mu_\theta(x_t, t) + \frac{\lambda_{t-1}\sigma_t^2}{\alpha}\nabla_{x_t}\hat{r}(x_t), \tag{12}$$

where $\mu_\theta(x_t, t)$ denotes the base model's predicted mean, σ_t^2 is the noise variance at timestep t, α is the KL regularization weight, and λ_{t-1} is a time-dependent scaling factor defined by the exponential schedule $\lambda_t = (1+\gamma)^{t-1}$ with $\gamma = 0.024$, as introduced in Kim et al. (2025). The reward

function is defined as $\hat{r}(x_t) = r(x_0(x_t))$, where $x_0(x_t)$ denotes the Tweedie approximation-based reconstructed image obtained from x_t using the denoiser network.

We adapted this approach to the multi-objective setting by combining gradients from two reward functions r_1 and r_2 as,

$$\nabla_{x_t}\hat{r}(x_t) = w_1\nabla_{x_t}r_1(x_0(x_t)) + (1-w_1)\nabla_{x_t}r_2(x_0(x_t)). \tag{13}$$

However, to ensure that the influence of each reward is independent of its scale or gradient magnitude, we normalized the individual gradients before combining them,

$$\nabla_{x_t}\hat{r}(x_t) = w_1\frac{\nabla_{x_t}r_1(x_0(x_t))}{\|\nabla_{x_t}r_1(x_0(x_t))\|} + (1-w_1)\frac{\nabla_{x_t}r_2(x_0(x_t))}{\|\nabla_{x_t}r_2(x_0(x_t))\|}. \tag{14}$$

This normalization ensures that the reward guidance strength is controllable and not biased by the nature or scale of individual rewards.

CoDe: Introduced by Singh et al. (2025), CoDe is a gradient-free guidance method for aligning diffusion models with downstream reward functions. CoDe operates by partitioning the denoising process into blocks and, at each block, generating multiple candidate samples. It then selects the sample with the highest estimated lookahead reward to proceed with the next denoising steps. For our experiments, we configured CoDe with 20 particles and a lookahead of 5 steps.

B.2 Pseudo Code

In this section, we present the pseudo-code for the three inference-time algorithms introduced in section 4: DB-MPA, DB-KL, DB-MPA-LS. All algorithms leverage the approximation result from lemma 1 or proposition 2 to enable controllable sampling without requiring additional fine-tuning at inference time.

Algorithm 1 outlines the DB-MPA procedure, in which a user-specified preference vector w is used to linearly combine the drift functions of m RL fine-tuned models, each optimized independently for a distinct reward basis. Algorithm 2 presents the DB-KLA procedure, which instead blends the drift of a fine-tuned model with the pre-trained model. Algorithm 3 approximates Algorithm 1 by sampling a drift with the assigned preference weights. All fine-tuned models used in algorithms are obtained by applying the single-reward RL fine-tuning algorithm individually to each reward function.

Note that all algorithms adopt a basic Euler-Maruyama discretization to simulate the reverse SDE in eq. (5). In practice, this integration step can be replaced by any diffusion model's reverse process (e.g., DDIM (Song et al., 2020) or other solvers), as long as the drift term (or the predicted denoising output) is appropriately mixed.

Algorithm 1 DB-MPA

Input: RL-fine-tuned drifts $\{f^{(r_i,\alpha)}\}_{i=1}^m$; weights $w \in \mathbb{R}^m$, $\sum_{i=1}^m w_i = 1$; time grid $0 = t_0 < t_1 < \cdots < t_N = T$

Sample $x_{t_N} \sim \mathcal{N}(0, I)$
for $k \leftarrow N$ **down to** 1 **do**
  $\Delta t_k \leftarrow t_k - t_{k-1}$ ▷ positive
  noise $z \sim \mathcal{N}(0, I)$
  $f_{\text{mix}} \leftarrow \sum_{i=1}^m w_i\, f^{(r_i,\alpha)}(x_{t_k}, t_k)$
  $x_{t_{k-1}} \leftarrow x_{t_k} - f_{\text{mix}}\,\Delta t_k + \sigma(t_k)\sqrt{\Delta t_k}\, z$
end for

Output: x_{t_0}

B.3 Prompt sets

We evaluate our methods on two datasets: *Short-DrawBench* and *GenEval*.

Short-DrawBench. The original DrawBench dataset (Saharia et al., 2022b) contains 183 prompts across 11 categories. For our experiments, we isolate the 25 prompts in the `color` category, forming

Algorithm 2 DB-KLA

Input: RL-fine-tuned drift $f^{(r,\alpha)}$; original pretrained drift f^{pre}; KL-reweight parameter $\lambda \geq 0$; time grid $0 = t_0 < t_1 < \cdots < t_N = T$

Sample $x_{t_N} \sim \mathcal{N}(0, I)$
for $k \leftarrow N$ **down to** 1 **do**
  $\Delta t_k \leftarrow t_k - t_{k-1}$ ▷ positive
  noise $z \sim \mathcal{N}(0, I)$
  $f_{\text{KL}} \leftarrow \lambda f^{(r,\alpha)}_{t_k}(x_{t_k}, t_k) + (1-\lambda) f^{pre}_{t_k}(x_{t_k}, t_k)$
  $x_{t_{k-1}} \leftarrow x_{t_k} - f_{\text{KL}}\, \Delta t_k + \sigma(t_k)\sqrt{\Delta t_k}\, z$
end for
Output: x_{t_0}

Algorithm 3 DB-MPA-LS

Input: RL-fine-tuned drifts $\{ f^{(r_i,\alpha)}\}_{i=1}^m$; weights $w \in \mathbb{R}^m$, $\sum_{i=1}^m w_i = 1$; time grid $0 = t_0 < t_1 < \cdots < t_N = T$

Sample $x_{t_N} \sim \mathcal{N}(0, I)$
for $k \leftarrow N$ **down to** 1 **do**
  $\Delta t_k \leftarrow t_k - t_{k-1}$ ▷ positive
  noise $z \sim \mathcal{N}(0, I)$
  sample i_k from $\{1, 2, \ldots, m\}$ with probability $(w_1, w_2, \ldots, w_m)$
  $x_{t_{k-1}} \leftarrow x_{t_k} - f^{(r_{i_k},\alpha)}(x_{t_k}, t_k)\, \Delta t_k + \sigma(t_k)\sqrt{\Delta t_k}\, z$
end for
Output: x_{t_0}

the *Short-DrawBench* subset. This reduced scale enables direct comparison with MORL, since training separate models for each preference or KL weight is computationally feasible. To test generalization, we further construct a set of 1,000 evaluation prompts generated by GPT-4 (Achiam et al., 2023). These prompts introduce novel object–color and multi-object compositions not present in the training subset. The instruction used for generating this test set was:

"Please generate 1000 testing prompts that are similar to the following training prompts, which are color+object combinations. You should use colors that appeared in the train set or have a similar semantic meaning. Objects can be a little more common or random."

GenEval. The GenEval benchmark (Kirstain et al., 2023) consists of 550 prompts designed to test compositional generalization, spanning attributes such as color, counting, spatial relations, and multi-object scenes. In addition to the official prompts, we generate an extra 700 held-out evaluation prompts using the official GenEval prompt generation toolkit. These follow the same construction rules as the original dataset, obtained by varying random seeds and object/color assignments.

B.4 Computing Hardware and Hyperparameters

Fine-tuning of Stable Diffusion for each KL weight and reward composition was performed on NVIDIA A100 GPUs using mixed precision. We used the AdamW optimizer with a learning rate of 1×10^{-5} for policy updates and applied LoRA with rank 4. Gradient accumulation was set to 12, with a per-GPU batch size of 2 for policy updates and 6 for prompt sampling.

Policy updates followed a clipped PPO-style objective with a clipping ratio of 1×10^{-4} following Fan et al. (2023). Each outer iteration performed 5 policy gradient steps and 5 value function updates (batch size 256, learning rate 1×10^{-4}), using a replay buffer of size 1000.Training required approximately 96,000 online samples to converge for the *Short-DrawBench* subset. A similar size of online samples is used for GenEval.

C DB-MPA Algorithm: Additional Results

In this section, we present additional experimental results for the DB-MPA algorithm. We begin with reward evaluations on the training prompts. Next, we demonstrate that DB-MPA naturally

extends to alignment with three rewards ($m = 3$). We also show that DB-MPA-LS produces outputs visually close to DB-MPA. We then provide additional qualitative comparisons with baselines to further highlight DB-MPA's effectiveness. Finally, we evaluate DB-MPA's ability to achieve fine-grained multi-preference alignment.

C.1 Results on Training Prompts

For the *Short-DrawBench* setting, Table 2 reports the performance of DB-MPA and baseline algorithms relative to Stable Diffusion, evaluated on the training prompts (30 random seed per prompt, 750 images in total). Across all preference weights, DB-MPA consistently outperforms RS, CoDe, and RGG.

We next consider the *GenEval* dataset, which evaluates compositional generalization. Table 3 reports the reward improvements of all methods relative to Stable Diffusion. DB-MPA and DB-MPA-LS achieve the best or near-best gains across most preference weights. Although the table lists separate Δr_1 and Δr_2, we also computed the weighted reward $\Delta\mathrm{WR} = wr_1 + (1-w)r_2$. On this aggregate metric, DB-MPA and DB-MPA-LS consistently outperform all other baselines, confirming their superior trade-off performance.

Table 2: Quantitative comparison of DB-MPA and baseline methods on train prompts. Here $\Delta r_i = r_i - r_i^{\mathrm{SD}}$

		DB-MPA		**RS**		**CoDe**		**RGG**	
		Δr_1	Δr_2	Δr_1	Δr_2	Δr_1	Δr_2	Δr_1	Δr_2
Improvement (↑)	w=0.2	**0.19**	**0.74**	-0.01	0.61	0.14	0.23	0.12	0.59
	w=0.5	**0.49**	**0.50**	0.12	0.20	0.29	0.19	0.13	0.39
	w=0.8	**0.65**	**0.18**	0.54	0.02	0.34	0.12	0.03	0.16

Table 3: GenEval train results: reward improvements (Δr) relative to Stable Diffusion.

		DB-MPA		**DB-MPA-LS**		**RS**		**CoDe**		**RGG**	
		Δr_1	Δr_2	Δr_1	Δr_2	Δr_1	Δr_2	Δr_1	Δr_2	Δr_1	Δr_2
Reward (↑)	w=0.2	+0.122	**+0.497**	+0.143	+0.477	-0.021	+0.378	**+0.254**	+0.107	+0.064	+0.497
	w=0.5	+0.267	**+0.357**	**+0.376**	+0.310	+0.161	+0.192	+0.344	+0.067	+0.104	+0.327
	w=0.8	+0.382	**+0.185**	**+0.411**	+0.180	+0.340	+0.089	+0.374	+0.007	-0.246	+0.111

C.2 Quantitative Results on GenEval Test Data

Table 4 reports the raw numerical values corresponding to fig. 5 shown in the main paper.

Table 4: GenEval (test): numerical results (r_1, r_2) corresponding to the Pareto-front plot fig. 5 in the main text. DB-MPA and DB-MPA-LS consistently dominate baselines across preference weights.

		SD		**DB-MPA**		**DB-MPA-LS**		**RS**		**CoDe**		**RGG**	
		r_1	r_2	r_1	r_2	r_1	r_2	r_1	r_2	r_1	r_2	r_1	r_2
Reward (↑)	w=0	-0.15	-0.08	-0.17	0.57	-0.17	0.57	-0.17	0.57	-0.03	0.07	0.03	0.52
	w=0.2	-0.15	-0.08	0.01	0.50	-0.08	0.54	-0.13	0.41	-0.07	0.05	0.02	0.44
	w=0.5	-0.15	-0.08	0.23	0.36	0.16	0.43	-0.01	0.19	0.05	0.01	-0.35	0.27
	w=0.8	-0.15	-0.08	0.35	0.20	0.29	0.22	0.28	0.10	0.12	-0.05	-0.41	0.10
	w=1	-0.15	-0.08	0.35	0.11	0.35	0.11	0.35	0.11	0.12	-0.09	-0.20	-0.06

C.3 Results for Conflicting Rewards

To evaluate DB-MPA under adversarial objectives, we consider the conflict between *JPEG compressibility* and *VILA aesthetics*. The JPEG reward incentivizes smooth, low-detail images, whereas

VILA prioritizes fine-grained, high-quality visuals. These objectives are naturally at odds: optimizing for JPEG typically harms aesthetics. For example, while the Stable Diffusion (SD) baseline scores $r_1 = -0.09$ on JPEG and $r_2 = 0.48$ on VILA, an RL-fine-tuned JPEG model attains $r_1 = 1.52$ but drops to $r_2 = -0.40$.

We train a JPEG-aligned model (r_1) and combine it with our VILA-aligned model (r_2) using DB-MPA. Because JPEG compressibility is non-differentiable, gradient-based methods such as RGG cannot be applied. We therefore compare DB-MPA against Rewarded Soup (RS) and CoDe. Rewards are reported as a function of the blending weight $w \in [0, 1]$, with $w = 1$ preferring JPEG and $w = 0$ preferring VILA.

Across all weights, DB-MPA achieves substantially higher weighted rewards than both RS and CoDe. This demonstrates that DB-MPA can effectively balance two strongly conflicting objectives far better than competing baselines.

Table 5: Performance on Short-drawbench test prompts under conflicting rewards: JPEG compressibility (r_1) and VILA aesthetics (r_2). We also report the weighted reward $\mathrm{WR} = wr_1 + (1-w)r_2$. The best weighted reward is bold.

		DB-MPA			**RS**			**CoDe**		
		r_1	r_2	WR	r_1	r_2	WR	r_1	r_2	WR
Reward (↑)	w=0.2	0.52	0.40	**0.44**	0.11	0.28	0.21	0.04	0.02	0.03
	w=0.5	1.00	0.18	**0.59**	0.30	0.02	0.16	0.22	0.03	0.12
	w=0.8	1.35	-0.18	**0.88**	0.93	-0.13	0.72	0.37	-0.01	0.29

C.4 Effect of Increasing the Number of Rewards

We study how the performance of DB changes as the number of reward models increases. In Figure fig. 7, we evaluate DB under 2-, 3-, and 4-reward settings and compare DB-MPA, DB-MPA-LS, and RS, all of which interpolate the same set of finetuned reward-basis models. It can be observed that the improvements of DB-MPA and DB-MPA-LS over the pretrained model remain stable as more rewards are introduced. All experiments use uniform average weights. From table 6, we observe that DB-MPA achieves the largest improvement, while DB-MPA-LS performs slightly worse but reduces inference cost to essentially the same unit-time speed as SD v1.5. In contrast, the baseline RS, despite interpolating the same 2–4 reward-basis models, performs substantially worse than DB, and its performance degrades noticeably as the number of rewards increases.

Figure 7: Performance comparison of DB-MPA and baseline algorithms under different numbers of reward models. R1 = ImageReward, R2 = VILA, R3 = Compressibility, R4 = PickScore. Performance improvement is computed as (algorithm reward) - (SD-v1.5 reward). DB-MPA and DV-MPA-LS consistently outperform RS as the number of rewards increases.

Table 6: Performance improvements under 2, 3, and 4 reward settings. Each column shows $\Delta r_i = r_i^{\text{method}} - r_i^{\text{SDv1.5}}$, and the group-wise mean.

	2-Reward			3-Reward				4-Reward				
Method	Δr_1	Δr_2	Avg	Δr_1	Δr_2	Δr_3	Avg	Δr_1	Δr_2	Δr_3	Δr_4	Avg
DB	0.54	**0.38**	**0.46**	0.30	**0.29**	**0.75**	**0.45**	**0.40**	0.22	**0.62**	**0.39**	**0.41**
LS	**0.58**	0.31	0.45	**0.37**	0.26	0.56	0.39	0.37	**0.28**	0.50	0.38	0.38
RS	0.15	0.13	0.14	-0.00	0.08	0.14	0.07	0.03	0.05	0.10	0.03	0.05

C.5 Results for Three-Reward Setting

To evaluate DB-MPA in a more complex multi-objective setting, we conducted experiments using three distinct reward functions: ImageReward for text-image alignment, VILA for aesthetic quality, and PickScore Kirstain et al. (2023) as a proxy for human preference. Figure 8 illustrates DB-MPA performance across various weight combinations in the three-reward setting. DB-MPA consistently adapts its outputs to reflect user-specified preferences, demonstrating scalable control without requiring additional retraining.

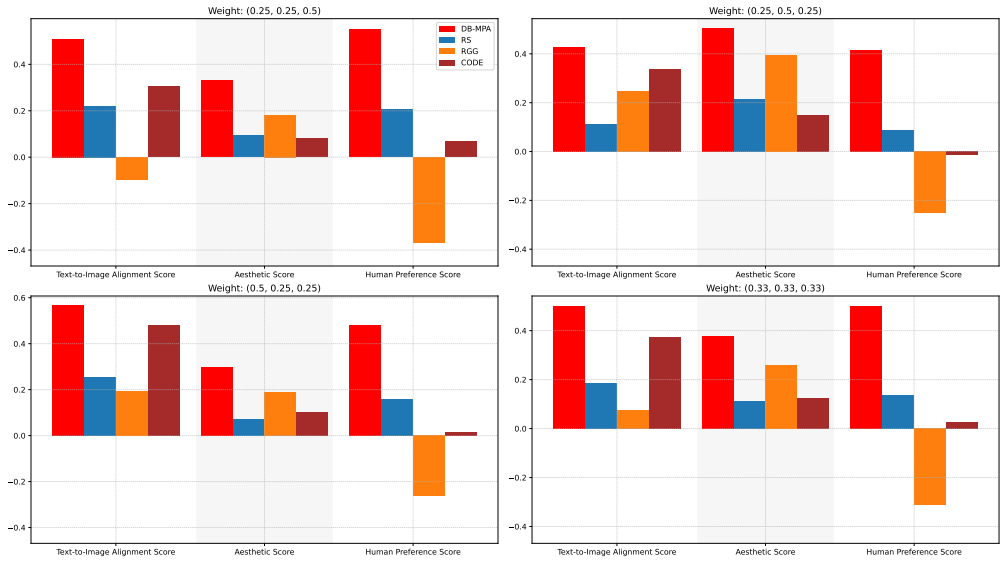

Figure 8: Performance comparison of DB-MPA and baseline algorithms in the $m = 3$ rewards setting, using ImageReward (text-image alignment), VILA (aesthetic quality), and PickScore (human preference). Each bar shows the improvement over SDv1.5 for the corresponding reward. DB-MPA consistently outperforms all baselines across different weight combinations and all reward dimensions.

C.6 Extension to SDXL

To examine whether the preference trade-off behavior observed in SD 1.5 carries over to a substantially larger backbone, we extend our experiments to Stable Diffusion XL (SDXL). The SDXL base UNet contains 1.6B parameters, more than 5× larger than the 300M UNet in SD 1.5, and the full SDXL pipeline totals approximately 2.6B parameters. Following seminal RL works on fine-tuning diffusion model Fan et al. (2023); Black et al. (2024) that train and validate on a single prompt, we also fine-tune SDXL on the prompt ("an orange colored sandwich"). As in the SD-1.5 setup, we use two reward models—ImageReward (alignment) and VILA (aesthetics). The corresponding training reward curves are shown in Figure 9.

After training, we evaluated the model across different preference weights. For DB-MPA, DB-MPA-LS, and two baselines RS and CoDe, we swept w in increments of 0.1. For RGG, due to it huge inference time cost, we only evaluated five points: $w \in \{0, 0.2, 0.5, 0.7, 1.0\}$. For each point, 64 random seeds are used. The resulting Pareto front is shown in Figure 10. Table 7 reports

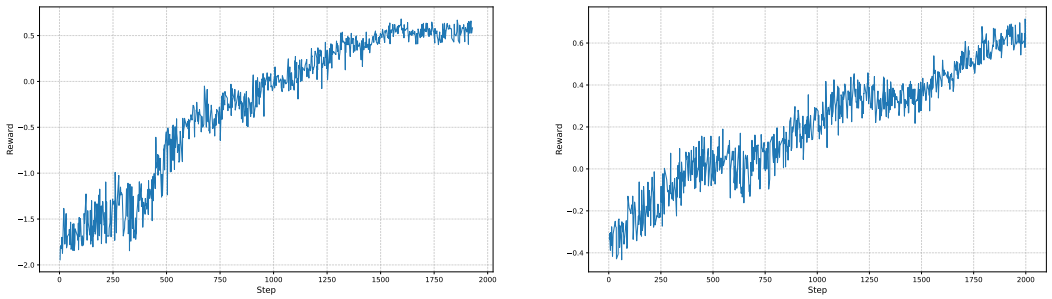

(a) ImageReward training curve.

(b) VILA training curve.

Figure 9: SDXL training curves for the two reward models. Training was run for roughly 2000 epochs over 72 GPU(A100) hours.

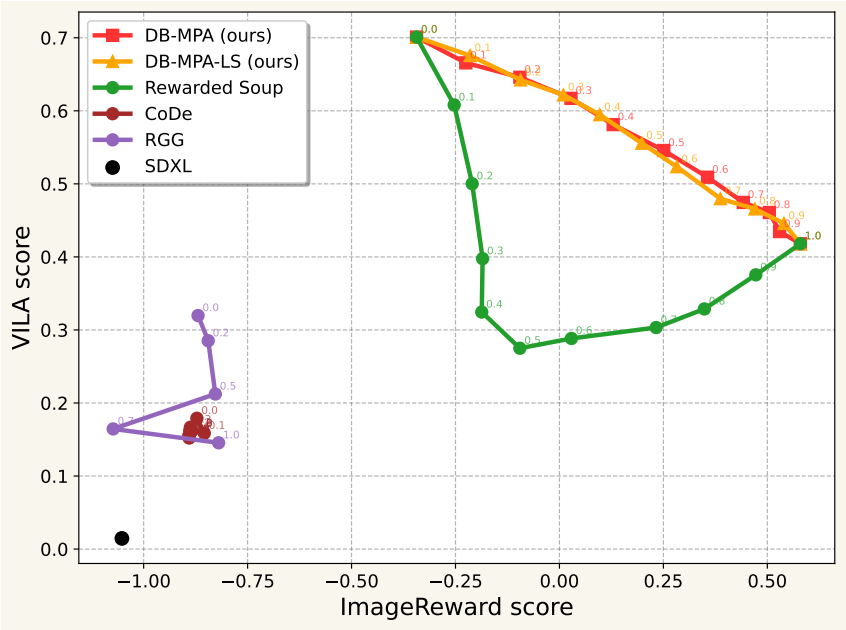

Figure 10: Pareto front of the SDXL LoRA model across preference weights.

the numerical results for the representative weights. The qualitative trends are consistent with our observations in SD 1.5: DB-MPA and DB-MPA-LS continue to provide controllable reward trade-offs in the SDXL setting, achieving larger performance improvements compared to other baselines. Training-based methods (DB-MPA, DB-MPA-LS, and RS) demonstrate superior performance over training-free approaches (RGG and CoDe). Notably, CoDe exhibits similar performance across different reward weightings, which may be attributed to SDXL's larger VAE being more sensitive to noise in the intermediate-step predicted images during CoDe's lookahead best-of-N sampling scheme.

C.7 Visual Similarity of DB-MPA and DB-MPA-LS

We present visual comparisons among DB-MPA, DB-MPA-LS, and RS under the two-reward setting using ImageReward (text-image alignment) and VILA (aesthetic quality). The results indicate that, for interpolating the same pair of diffusion reverse processes, DB-MPA and DB-MPA-LS yield visually similar outputs, both surpassing the baseline RS in image quality.

Table 7: SDXL single prompt results: r_1 = ImageReward, r_2 = VILA. The pretrained SDXL has: $r_1 = -1.05$, $r_2 = 0.01$.

		DB-MPA		DB-MPA-LS		RS		CoDe		RGG	
		r_1	r_2	r_1	r_2	r_1	r_2	r_1	r_2	r_1	r_2
Reward (↑)	w=0.0	−0.34	0.70	−0.34	0.70	−0.34	0.70	−0.87	0.18	−0.87	0.32
	w=0.2	−0.10	0.65	−0.09	0.64	−0.21	0.50	−0.89	0.16	−0.84	0.29
	w=0.5	0.25	0.55	0.20	0.56	−0.10	0.27	−0.89	0.16	−0.83	0.21
	w=0.7	0.44	0.47	0.39	0.48	0.23	0.30	−0.89	0.15	−1.07	0.16
	w=1.0	0.58	0.42	0.58	0.42	0.58	0.42	−0.88	0.16	−0.82	0.15

Figure 11: w denotes the weight assigned to ImageReward, with $1 - w$ corresponding to the weight for VILA. Both DB-MPA and DB-MPA-LS produce visually similar results, and each generates images better aligned to the user's preference than the baseline RS.

C.8 Visual Comparison with Baselines

We provide additional qualitative comparisons between DB-MPA and the baselines in fig. 12 using prompts from both the train and test sets, for $w \in \{0.2, 0.5, 0.8\}$. Despite requiring no extra fine-tuning, DB-MPA generates images that are visually close to the MORL oracle baseline, and outperforms all other baseline methods.

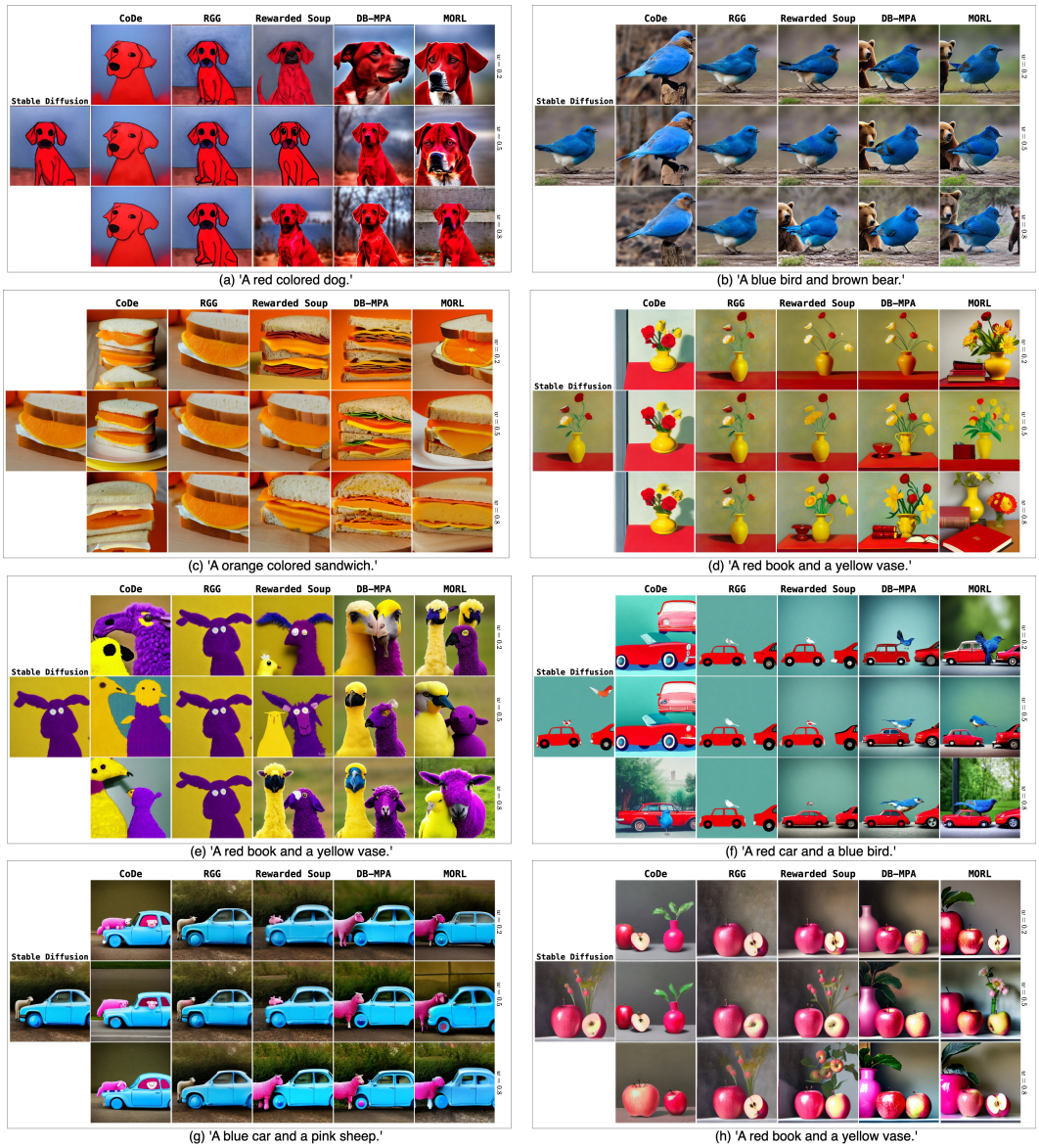

(a) 'A red colored dog.' (b) 'A blue bird and brown bear.'

(c) 'A orange colored sandwich.' (d) 'A red book and a yellow vase.'

(e) 'A red book and a yellow vase.' (f) 'A red car and a blue bird.'

(g) 'A blue car and a pink sheep.' (h) 'A red book and a yellow vase.'

Figure 12: Qualitative comparison of DB-MPA with baselines. Subfigures (a)–(d) correspond to training prompts, and (e)–(h) to test prompts. In several cases, such as (a) and (e), Stable Diffusion produces cartoonish or unrealistic outputs. In contrast, DB-MPA generates more realistic and semantically aligned images by effectively leveraging multi-reward alignment, without requiring any additional fine-tuning.

C.9 Multi-Preference Alignment with Finer Granularity

In Fig. 13, we present additional results of DB-MPA and RS for multi-preference alignment with finer granularity of w, with $w \in \{0.1, 0.2, \ldots, 0.9\}$. As observed, both algorithms exhibit a smooth transition from aesthetically pleasing results to outputs that are more aligned with the input prompt. However, DB-MPA typically achieves better alignment with the input prompt, especially for $w \in [0.3, 0.7]$.

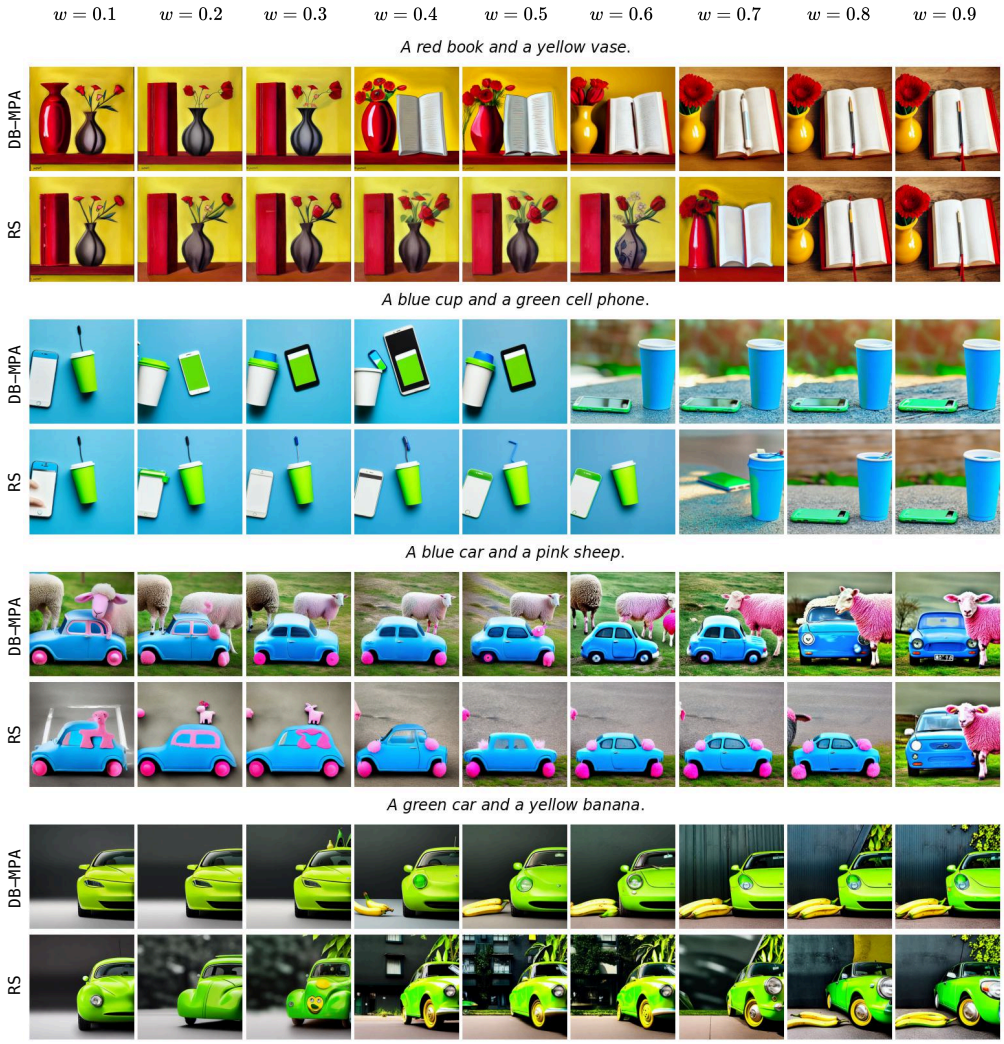

Figure 13: Qualitative comparison between DB-MPA (first row) and RS (second row) with ImageReward and aesthetic score as rewards. Each block shows generations as the ImageReward weight w increases from 0.1 to 0.9 (left to right). The first two examples are from the training prompt set, and the last two from the test prompt set. DB-MPA demonstrates smoother transitions and more precise alignment with the target reward preferences compared to RS, supporting the trends observed in the quantitative results.

D DB-KLA: Additional Results

This section presents additional results for DB-KLA, including qualitative comparisons with the MORL oracle across diverse prompts. It also evaluates DB-KLA's controllability under fine-grained variations of the KL weight.

D.1 Qualitative Comparison with Baselines

We provide additional qualitative comparisons between DB-KLA and the MORL oracle baseline in fig. 14, using prompts from both the train and test sets. These examples show how DB-KLA adapts generation quality as the KL regularization strength changes, producing outputs that closely resemble those of the oracle baseline.

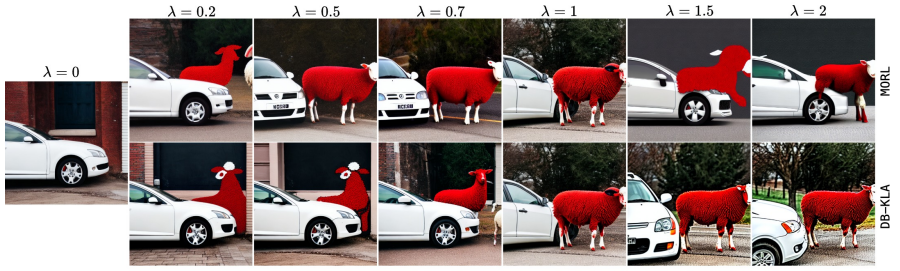

(a) 'A white car and a red sheep.'

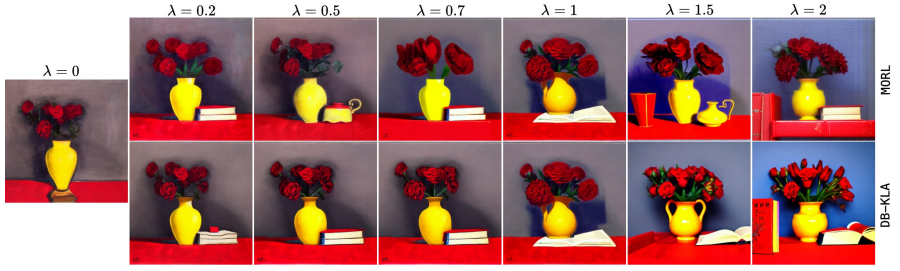

(b) 'A red book and a yellow vase.'

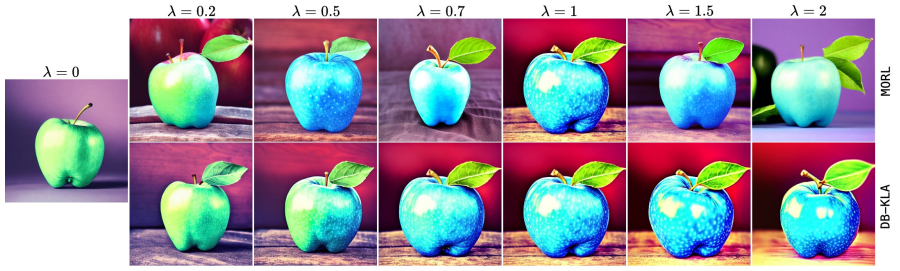

(c) 'A blue colored apple.'

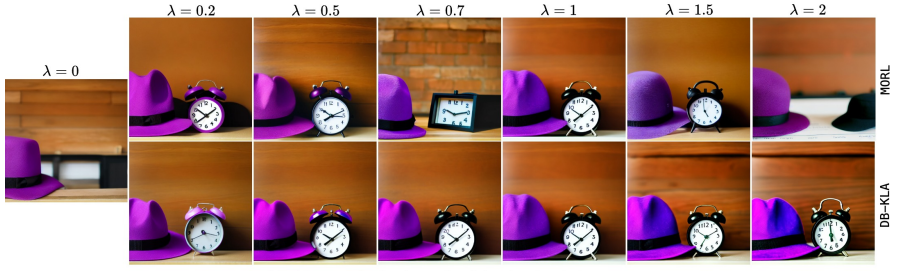

(d) 'A purple hat and a black clock.'

Figure 14: Qualitative comparison between DB-KLA and MORL for KL weights $\lambda \in \{0.2, 0.5, 0.7, 1.0, 1.5, 2.0\}$. The first two rows show the results with train prompts, and the last two show the results with test prompts. DB-KLA generates images of similar quality to those of the MORL oracle baseline without any additional fine-tuning.

D.2 KL Alignment with Finer Granularity

In Fig. 15, we present additional results of DB-KLA with finer granularity of λ, for $\lambda = [0, 0.2, 0.5, 0.7, 1.0, 1.5, 2.0]$. As regularization increases, the model shifts more toward optimizing the text-to-image reward, producing images that better match the prompt but drift further from the original Stable Diffusion output.

Figure 15: KL weight alignment in DB for $\lambda = [0, 0.2, 0.5, 0.7, 1.0, 1.5, 2.0]$, with λ increasing from left to right.

E Impact Statement

Diffusion Blend enables flexible, inference-time alignment of diffusion models with user-specified preferences over multiple reward objectives and regularization strengths, without additional fine-tuning. This significantly reduces computational costs and increases adaptability for personalization. By leveraging a small set of fine-tuned models, it opens the door to scalable, user-controllable generative AI and sets the stage for more preference-aware deployment. While our work has broad implications for AI alignment and deployment as it enhances the existing diffusion models' performance, we do not foresee any immediate societal concerns that require specific highlighting.

F THE USE OF LARGE LANGUAGE MODELS

Portions of this work were prepared with the assistance of a large language model (ChatGPT, GPT-5, by OpenAI). The model was used as a writing assistant to improve clarity, grammar, and organization of the manuscript, and to suggest alternative phrasings of technical content written by the authors. All ideas, experiments, analyses, and final decisions regarding the content remain the responsibility of the authors. The test prompt set for the Drawbench prompt dataset is generated by LLM, following the standard benchmark like GenEval. The model was not used to generate research ideas, perform experiments, or create unverifiable scientific claims.